

2.15
9/11/67
ANL-7270

ANL-7270

MASTER

Argonne National Laboratory

ANALYSIS OF
HIGH CONVERSION CRITICAL EXPERIMENTS

by

E. M. Pennington

DISCLAIMER

This report was prepared as an account of work sponsored by an agency of the United States Government. Neither the United States Government nor any agency Thereof, nor any of their employees, makes any warranty, express or implied, or assumes any legal liability or responsibility for the accuracy, completeness, or usefulness of any information, apparatus, product, or process disclosed, or represents that its use would not infringe privately owned rights. Reference herein to any specific commercial product, process, or service by trade name, trademark, manufacturer, or otherwise does not necessarily constitute or imply its endorsement, recommendation, or favoring by the United States Government or any agency thereof. The views and opinions of authors expressed herein do not necessarily state or reflect those of the United States Government or any agency thereof.

DISCLAIMER

Portions of this document may be illegible in electronic image products. Images are produced from the best available original document.

The facilities of Argonne National Laboratory are owned by the United States Government. Under the terms of a contract (W-31-109-Eng-38) between the U. S. Atomic Energy Commission, Argonne Universities Association and The University of Chicago, the University employs the staff and operates the Laboratory in accordance with policies and programs formulated, approved and reviewed by the Association.

MEMBERS OF ARGONNE UNIVERSITIES ASSOCIATION

The University of Arizona	The University of Iowa	Northwestern University
Carnegie Institute of Technology	Kansas State University	University of Notre Dame
Case Institute of Technology	The University of Kansas	The Ohio State University
The University of Chicago	Loyola University	Purdue University
University of Cincinnati	Marquette University	Saint Louis University
Illinois Institute of Technology	Michigan State University	Washington University
University of Illinois	The University of Michigan	Wayne State University
Indiana University	University of Minnesota	The University of Wisconsin
Iowa State University	University of Missouri	

LEGAL NOTICE

This report was prepared as an account of Government sponsored work. Neither the United States, nor the Commission, nor any person acting on behalf of the Commission:

- A. Makes any warranty or representation, expressed or implied, with respect to the accuracy, completeness, or usefulness of the information contained in this report, or that the use of any information, apparatus, method, or process disclosed in this report may not infringe privately owned rights; or
- B. Assumes any liabilities with respect to the use of, or for damages resulting from the use of any information, apparatus, method, or process disclosed in this report.

As used in the above, "person acting on behalf of the Commission" includes any employee or contractor of the Commission, or employee of such contractor, to the extent that such employee or contractor of the Commission, or employee of such contractor prepares, disseminates, or provides access to, any information pursuant to his employment or contract with the Commission, or his employment with such contractor.

Printed in the United States of America

Available from

Clearinghouse for Federal Scientific and Technical Information
National Bureau of Standards, U. S. Department of Commerce
Springfield, Virginia 22151

Price: Printed Copy \$3.00; Microfiche \$0.65

ANL-7270
Reactor Technology
(TID-4500)
AEC Research and
Development Report

ARGONNE NATIONAL LABORATORY
9700 South Cass Avenue
Argonne, Illinois 60439

CESTI PRICES

H.C. \$ 3.00, MN 165

ANALYSIS OF
HIGH CONVERSION CRITICAL EXPERIMENTS

by

E. M. Pennington

Reactor Physics Division

March 1967

LEGAL NOTICE

This report was prepared as an account of Government sponsored work. Neither the United States, nor the Commission, nor any person acting on behalf of the Commission:

A. Makes any warranty or representation, expressed or implied, with respect to the accuracy, completeness, or usefulness of the information contained in this report, or that the use of any information, apparatus, method, or process disclosed in this report may not infringe privately owned rights; or

B. Assumes any liabilities with respect to the use of, or for damages resulting from the use of any information, apparatus, method, or process disclosed in this report.

As used in the above, "person acting on behalf of the Commission" includes any employee or contractor of the Commission, or employee of such contractor, to the extent that such employee or contractor of the Commission, or employee of such contractor prepares, disseminates, or provides access to, any information pursuant to his employment or contract with the Commission, or his employment with such contractor.

2

THIS PAGE
WAS INTENTIONALLY
LEFT BLANK

TABLE OF CONTENTS

	<u>Page</u>
ABSTRACT	7
I. INTRODUCTION	7
II. FUEL, CLADDING, AND LATTICE DESCRIPTIONS	9
III. CALCULATION OF THERMAL PARAMETERS	11
IV. CALCULATION OF NONTHERMAL PARAMETERS	18
V. CRITICALITY CALCULATIONS	23
VI. RADIAL REFLECTOR SAVINGS	26
VII. MICROPARAMETER CALCULATIONS	27
A. Initial and Modified Conversion Ratios and α^{25}	27
B. U^{238} Capture Cadmium Ratios	28
C. U^{235} Fission Cadmium Ratios	29
D. Gold and Indium Cadmium Ratios	29
E. U^{238} -to- U^{235} Fission Ratios	32
VIII. EFFECTS OF CROSS-SECTION CHANGES ON REACTIVITY	38
IX. DISCUSSION AND CONCLUSIONS	39
REFERENCES	41

LIST OF FIGURES

<u>No.</u>	<u>Title</u>	<u>Page</u>
1.	Experimental and Theoretical Thermal Disadvantage Factors in Hi-C Cores	16
2.	Theoretical and Experimental Bucklings	24
3.	Two-group Parameters for Hi-C Aluminum-clad Lattices	25
4.	Conversion Ratios for Hi-C Stainless Steel-clad Cores	28
5.	U^{238} Epicadmium to Subcadmium Capture Ratios for Hi-C Stainless Steel-clad Cores	29
6.	U^{235} Fission Cadmium Ratios for Hi-C Stainless Steel-clad Cores	30
7.	U^{238} -to- U^{235} Fission Ratios for Hi-C Stainless Steel-clad Cores	34

LIST OF TABLES

No.	Title	Page
I.	Hi-C and BORAX-V Fuel and Cladding Data	9
II.	Hi-C and BORAX-V Lattice Descriptions	10
III.	Thermal-flux and Neutron-number-density Ratios and Average Velocities	13
IV.	Thermal Parameters Based on Nelkin-kernel THERMOS Problems	13
V.	Comparisons of Thermal Quantities Based on Various Scattering Kernels for Hydrogen	14
VI.	Thermal-flux and Neutron-number-density Ratios for 27-group and 30-group Edits	14
VII.	B692/RP Problems for the H1.069ΔS Lattice.	15
VIII.	U ²³⁵ Fission Ratios for Lattices with Stainless Steel Cladding	16
IX.	Scattering Cross Sections Used in Dancoff-factor Calculations	19
X.	Dancoff Factors	19
XI.	Resonance Integrals from GAM-I Output.	20
XII.	Constants from GAM-I for Three Fast Groups in the P ₁ Approximation.	22
XIII.	A Comparison of P ₁ and B ₁ Constants from GAM-I.	22
XIV.	Buckles and Fluxes from Fundamental-mode Calculations.	24
XV.	Two-group Parameters	25
XVI.	Radial Reflector Savings	26
XVII.	Initial and Modified Conversion Ratios and α ²⁵	27
XVIII.	Calculated and Experimental Conversion Ratios.	28
XIX.	Calculated and Experimental U ²³⁸ Capture Cadmium Ratios .	28
XX.	Calculated and Experimental U ²³⁵ Fission Cadmium Ratios .	29
XXI.	Gold Cadmium Ratios	31
XXII.	Indium Cadmium Ratios.	31
XXIII.	U ²³⁸ -to-U ²³⁵ Fission Ratios.	34

LIST OF TABLES

No.	<u>Title</u>	<u>Page</u>
XXIV.	GAM-I Cross Sections Averaged over a Fission Spectrum from 1.35 to 10 MeV	35
XXV.	MUFT-4 Cross Sections Averaged over a Fission Spectrum from 1.35 to 10 MeV	35
XXVI.	Average Group 1 Fluxes Calculated Using GAM-I Fission-spectrum Cross Sections	36
XXVII.	Reactivity Changes on Substitution of Various Group 1 Cross Sections into Four-group BUCKLE Problems	37
XXVIII.	Effects of Cross-section Changes on Reactivity ($\Delta k_{\text{eff}}/k_{\text{eff}}$, %)	38

ANALYSIS OF HIGH CONVERSION CRITICAL EXPERIMENTS

by

E. M. Pennington

ABSTRACT

Critical experiments performed in the ZPR-7 facility using Hi-C or BORAX-V fuel and light-water moderator are analyzed. The Hi-C fuel consisted of 3.04 w/o enriched UO_2 pellets of 0.935 cm diameter, stacked to a height of 122 cm in either aluminum or stainless steel tubing. Experiments with BORAX-V fuel used UO_2 pellets, which were 4.95 w/o enriched, 0.871 cm in diameter, and stacked 61 cm high in stainless steel tubing. All lattices analyzed consisted of fuel rods uniformly spaced in either square or triangular arrays. The H-to- U^{238} atom ratios in the cores varied from roughly 4.6 to 0.5 so that investigations extended far into the undermoderated region. Calculations of critical bucklings, reflector savings, and various microparameters are compared with experimental values. Agreement with experiment is in general reasonably good, except for the U^{238} -to- U^{235} fission ratio.

I. INTRODUCTION

The High Conversion Critical Experiments Program (Hi-C) was initiated to extend the range of investigations of light-water-moderated, slightly enriched, uranium oxide cores to lower hydrogen-to- U^{238} atom ratios than had been studied previously. Uniform lattices having H-to- U^{238} atom ratios from about 4.6 to 0.5 were studied. These H-to- U^{238} atom ratios correspond to water-to-fuel volume ratios ranging from 1.5 to 0.16. The various H-to- U^{238} atom ratios were obtained by using square and triangular grids of different pitches, except for the tightest loading, which was achieved without gridwork.

As the name of the program suggests, tightly packed cores have high conversion ratios, which retard reactivity losses with fuel depletion and therefore lead to long core lifetimes. Also, heavily loaded cores have large surface areas available for heat transfer, thereby allowing high power densities. The close spacing of the rods is ultimately limited by lack of

space for coolant flow and structural support. Tightly packed zones can be used as driver zones surrounding cores of more conventional design, leading to a net increase in the conversion ratio of the system. Thus the study of highly undermoderated cores is of interest for design of light-water-moderated power reactors.

Two lattices were studied using the 4.95 w/o enriched UO_2 BORAX-V fuel. The other lattices consisted of the 3.04 w/o enriched UO_2 Hi-C fuel. Initially, approximately 3200 aluminum-clad and 2100 stainless steel-clad Hi-C fuel pins were available. Later, all but 400 stainless steel-clad fuel pins were dejacketed, the pellets being transferred to aluminum cladding. This enabled the achievement of criticality for tighter lattices with aluminum-clad fuel. Four uniform Hi-C lattices of aluminum-clad fuel and one of stainless steel-clad fuel attained criticality. In addition, one other Hi-C uniform lattice with aluminum-clad fuel and five others with stainless steel-clad fuel were investigated. In these cases, criticality was attained by surrounding the central core region by one or two driver regions. Often the region next to the central core consisted of aluminum-clad fuel with the same pitch as the stainless steel-clad fuel in the central region, while the second driver zone, when present, contained fuel more loosely spaced. Microparameter measurements (initial conversion ratio, thermal disadvantage factor, etc.) were made in the central zone. All cores were constructed in a tank roughly 2 m in diameter, which provided an effectively infinite radial light-water reflector. The water level in the tank could be adjusted to any desired level to achieve criticality.

Reference 1 describes in detail the ZPR-7 critical facility, the Hi-C and BORAX-V fuel pins and cladding, the experimental techniques involved, and the experimental results obtained. Some early Hi-C experimental results were presented at technical meetings.^{2,3} Later experimental work was described in Reactor Physics Division Annual Reports.^{4,5} Experimental studies of thermal disadvantage factors⁶ and cadmium ratios⁷ were also reported previously. References 8 and 9 have outlined some of the theoretical work. A short comparison of experimental and calculated results has also been presented.¹⁰

The next section of this report describes briefly the fuel, cladding, and lattice dimensions involved. Following sections describe the calculational methods in detail and present the numerical results. Most of the calculations were performed in the framework of four-group diffusion theory, constants for three fast groups being obtained from the GAM-I code,¹¹ and thermal group constants being derived from the THERMOS code.¹² Experimental and theoretical values are compared whenever possible.

II. FUEL, CLADDING, AND LATTICE DESCRIPTIONS

Table I presents data on the fuel and cladding dimensions and atomic number densities of these components, which were used in all calculations. The values in Table I are in substantial agreement with those quoted in Table III of Ref. 1. The number densities of hydrogen and oxygen in the light-water moderator were taken to be 0.06694×10^{24} and 0.03347×10^{24} atoms/cm³, respectively.

TABLE I. Hi-C and BORAX-V Fuel and Cladding Data

	BORAX-V	Hi-C
<u>Fuel</u>		
Enrichment, w/o	4.95	3.0422
Radius, cm	0.43561	0.46736
Length, cm	60.96	121.92
Oxide density, g/cm ³	10.2	10.2
²⁵ N, atoms/cm ³	0.001141×10^{24}	0.0007013×10^{24}
²⁸ N, atoms/cm ³	0.02163×10^{24}	0.02207×10^{24}
¹⁶ O, atoms/cm ³	0.04554×10^{24}	0.04554×10^{24}
<u>Cladding</u>		
Type	304 SS	6061-T6 Al
Inner radius, cm	0.43942	0.48445
Outer radius, cm	0.47752	0.52900
Density, g/cm ³	7.806	2.70
⁵⁶ Fe, atoms/cm ³	0.06063×10^{24}	0.06063×10^{24}
⁵² Cr, atoms/cm ³	0.01718×10^{24}	0.01718×10^{24}
⁶⁰ Ni, atoms/cm ³	0.00722×10^{24}	0.00722×10^{24}
²⁷ Al, atoms/cm ³	-	0.06025×10^{24}

Table II lists the volume fractions, unit-cell outer radii, H-to-U²³⁸ atom ratios, and H₂O-to-fuel volume ratios for all the Hi-C and BORAX-V uniform lattices. The core codes given in the first column of Table II will be used in referring to the lattices throughout the rest of this report.

TABLE II. Hi-C and BORAX-V Lattice Descriptions

Core Code	Lattice Pitch, cm	Fuel	Cladding	Unit-cell Radius, cm	Volume Fractions				H ₂ O/UO ₂ Volume Ratio	H/U ²³⁸ Atom Ratio
					Fuel	Void	Cladding	Water		
B1.27□S	1.27 square	BORAX-V	SS	0.71650	0.36963	0.00649	0.06805	0.55583	1.504	4.654
B1.27△S	1.27 triangular	BORAX-V	SS	0.66680	0.42679	0.00750	0.07857	0.48714	1.141	3.533
H1.349□A	1.349 square	Hi-C	Al	0.76109	0.37708	0.02808	0.07794	0.51690	1.371	4.158
H1.349□S	1.349 square	Hi-C	SS	0.76109	0.37708	0.02007	0.08504	0.51781	1.373	4.165
H1.24□A	1.24 square	Hi-C	Al	0.69960	0.44628	0.03323	0.09225	0.42824	0.9596	2.911
H1.24□S	1.24 square	Hi-C	SS	0.69960	0.44628	0.02376	0.10064	0.42932	0.9620	2.918
H1.27△A	1.27 triangular	Hi-C	Al	0.66680	0.49126	0.03658	0.10155	0.37061	0.7544	2.289
H1.27△S	1.27 triangular	Hi-C	SS	0.66680	0.49126	0.02615	0.11079	0.37180	0.7568	2.296
H1.166△A	1.166 triangular	Hi-C	Al	0.61220	0.58279	0.04340	0.12047	0.25334	0.4347	1.319
H1.166△S	1.166 triangular	Hi-C	SS	0.61220	0.58279	0.03103	0.13143	0.25475	0.4371	1.326
H1.127△A	1.127 triangular	Hi-C	Al	0.59172	0.62383	0.04646	0.12895	0.20076	0.3218	0.9760
H1.127△S	1.127 triangular	Hi-C	SS	0.59172	0.62383	0.03321	0.14069	0.20227	0.3242	0.9833
H1.069△S	1.069 triangular	Hi-C	SS	0.56127	0.69336	0.03691	0.15637	0.11336	0.1635	0.4959

III. CALCULATION OF THERMAL PARAMETERS

Thermal lattice parameters were computed with the aid of the THERMOS code¹² on the IBM-704. This code calculates the scalar thermal-neutron spectrum as a function of position in a lattice cell by solving numerically the integral transport equation with isotropic scattering. Thirty thermal groups and 20 space points are allowed in the code. Free-gas kernels are used, except for hydrogen, for which the Nelkin, Brown-St. John, and free-gas kernels are all available. The slowing-down source for the problems reported here was taken as resulting from hydrogen only, and was spatially flat in the H_2O region. The transport kernels in THERMOS are derived on the basis of mirror-image reflection at the cell boundary. Newmarch¹³ has shown that this boundary condition leads to a gross overestimate of the disadvantage factor in a cylindrical cell having a moderator region that is thin in terms of mean free paths. Thus the method of Honeck¹⁴ was used in which an extra region consisting of a heavy scatterer was placed outside the actual cell boundary. This method produces an essentially isotropic distribution of the neutrons returning to the actual cell. The extra region was three mean free paths thick in all problems. A mass of 10^5 amu was assigned to the heavy scatterer so that neutrons would be returned to the cell in the same velocity group in which they left. Since void regions are not allowed in this version of THERMOS, the inner radius of the cladding was set equal to the outer radius of the fuel, and the atomic number densities of the clad constituents were adjusted to yield the correct total number of atoms.

Calculations using the Nelkin kernel for hydrogen were carried out for all the lattices. Also, problems using both Brown-St. John and free-gas kernels for hydrogen were run for some lattices. The velocity limits for the 30 thermal groups were the same as those quoted in the THERMOS manual.¹² The cross-section library used was based on BNL-325 and the supplement.¹⁵ Since the upper velocity limit of Group 27 corresponds to an energy of 0.415 eV, which is almost exactly the same as the lower energy limit of 0.414 eV in GAM-I, edits were obtained for both 27 and 30 groups. (The group number in THERMOS increases with increasing velocity.) The upper energy limit of Group 30 is 0.785 eV. It is assumed that, above this limit, the flux per unit energy interval, $\phi(E)$, has a $1/E$ dependence.

In addition to the 30-group problems, THERMOS one-group calculations were done for all lattices using cross sections from the 27-group edits of the Nelkin-kernel multigroup problems. These one-group cross sections were also used in the three-region B692/RP collision probability code.^{16,17} This code assumes that neutrons incident on the boundary of the unit cell from the inside are returned isotropically. Average thermal fluxes are computed in B692/RP in the framework of the flat-flux approximation.

The thermal-diffusion coefficient is not calculated in the version of THERMOS used here. Thus a scheme was devised for its calculation. First the value of $(1 - \mu) \sigma_S$ for hydrogen in H_2O according to the Nelkin kernel was calculated from

$$\frac{(1 - \mu^H) \sigma_S^H}{\sum_{i=1}^{27} V_i N(V_i) \Delta V_i} = \frac{\sum_{i=1}^{27} (\sigma_{S0i}^H - \sigma_{S1i}^H) V_i N(V_i) \Delta V_i}{\sum_{i=1}^{27} V_i N(V_i) \Delta V_i}, \quad (1)$$

where V_i is the velocity of group i , which has a velocity interval of ΔV_i , $N(V_i)$ is the neutron number density of group i , and σ_{S0i}^H and σ_{S1i}^H are the P_0 and P_1 components of the hydrogen scattering cross section. Although the P_1 component is not used in THERMOS itself, it is calculated by the GAKER code, which is one of the THERMOS family of codes, and appears in the THERMOS library. The neutron number densities used in Eq. 1 were those for the outermost mesh interval in H_2O in the cell. A spatial average of $(1 - \mu^H) \sigma_S^H$ would differ little from the outer mesh-interval value. Values of $(1 - \mu) \sigma_S$ for all other materials were calculated simply as

$$(1 - \mu) \sigma_S = \left(1 - \frac{2}{3A}\right) \sigma_S,$$

where A is the mass number and σ_S is the constant, "high-energy," scattering cross section used in the free-gas kernel. The macroscopic values of $(1 - \mu) \Sigma_S$ were calculated for each cell region by summing the products of the microscopic $(1 - \mu) \sigma_S$ and the corresponding material number densities. Next the macroscopic values of $(1 - \mu) \Sigma_S$ for each cell region were flux-weighted using the 27-group edits of the Nelkin-kernel problems to yield the value of $(1 - \mu) \Sigma_S$ for the cell. Then Σ_{tr} for the cell was calculated as $\Sigma_{tr} = \Sigma_a + (1 - \mu) \Sigma_S$, where Σ_a is the absorption cross section of the 27-group edits. The diffusion constant was finally calculated from $D = 1/(3\Sigma_{tr})$, and the thermal-diffusion area was computed as $L^2 = D/\Sigma_a$.

A THERMOS Nelkin-kernel problem with one mesh interval was run for H_2O in order to yield values of Σ_a , D , and L^2 to be used in the radial reflector savings calculations described in Section VI.

Table III presents flux and neutron-number-density ratios for all the lattices based on the 27-group edits of the Nelkin-kernel problems. Average velocities are in dimensionless units based on 2200 m/sec. Flux ratios from the Nelkin and B692/RP one-group problems are given.

Subscripts 1, 2, and 3 in Table III denote fuel, cladding, and water regions, respectively. Reference 17 contains some of the flux ratios.

TABLE III. Thermal-flux and Neutron-number-density Ratios and Average Velocities

Quantity ^a	Description	Lattice												
		B1.27 \square S	B1.27 Δ S	H1.349 \square A	H1.349 \square S	H1.24 \square A	H1.24 \square S	H1.27 Δ A	H1.27 Δ S	H1.166 Δ A	H1.166 Δ S	H1.127 Δ A	H1.127 Δ S	H1.069 Δ S
$\bar{\phi}_2/\bar{\phi}_1$	Nelkin	1.1150	1.1124	1.0910	1.0837	1.0894	1.0819	1.0880	1.0807	1.0853	1.0781	1.0831	1.0772	1.0730
$\bar{\phi}_3/\bar{\phi}_1$	27-group	1.2535	1.2299	1.1737	1.1905	1.1572	1.1709	1.1486	1.1615	1.1286	1.1375	1.1271	1.1367	1.1167
\bar{n}_2/\bar{n}_1	Nelkin	1.1590	1.1565	1.1242	1.1143	1.1230	1.1129	1.1218	1.1116	1.1179	1.1077	1.1147	1.1057	1.0986
\bar{n}_3/\bar{n}_1	27-group	1.3554	1.3235	1.2411	1.2648	1.2184	1.2381	1.2063	1.2246	1.1774	1.1903	1.1729	1.1858	1.1570
\bar{v}_1 ^b	Nelkin	1.5900	1.6693	1.4922	1.5135	1.5788	1.6067	1.6507	1.6747	1.8120	1.8519	1.9151	1.9374	2.1446
\bar{v}_2	Nelkin	1.5295	1.6057	1.4481	1.4719	1.5314	1.5619	1.6009	1.6281	1.7593	1.8024	1.8607	1.8874	2.0946
\bar{v}_3	27-group	1.4703	1.5514	1.4112	1.4246	1.4995	1.5195	1.5719	1.5886	1.7371	1.7697	1.8403	1.8572	2.0699
$\bar{\phi}_2/\bar{\phi}_1$	Nelkin	1.1125	1.1105	1.0903	1.0829	1.0890	1.0815	1.0879	1.0807	1.0865	1.0789	1.0848	1.0785	1.0767
$\bar{\phi}_3/\bar{\phi}_1$	1-group	1.2462	1.2249	1.1696	1.1861	1.1551	1.1687	1.1477	1.1607	1.1299	1.1391	1.1299	1.1395	1.1233
$\bar{\phi}_2/\bar{\phi}_1$	B692/RP	1.1173	1.1142	1.0924	1.0859	1.0902	1.0836	1.0887	1.0824	1.0870	1.0801	1.0858	1.0798	1.0786
$\bar{\phi}_3/\bar{\phi}_1$	1-group	1.2394	1.2203	1.1641	1.1802	1.1497	1.1634	1.1413	1.1544	1.1299	1.1397	1.1260	1.1363	1.1334

^aSubscripts 1, 2, and 3 denote fuel, cladding, and water regions, respectively.

^bAverage velocities are in dimensionless units based on 2200 m/sec.

The thermal-flux ratios in Table III calculated by Nelkin 27-group, Nelkin one-group, or B692/RP one-group methods are all quite close to each other. Agreement between the Nelkin and B692/RP one-group calculations suggests that the use of the extra scattering region mocks up the isotropic return boundary condition well, and that the flat flux approximation is adequate for such closely packed lattices. Inspection of the velocities indicates the progressive hardening of the neutron spectrum as the H-to-U²³⁸ atom ratio is decreased.

Table IV lists thermal parameters for all the lattices, based on the Nelkin-kernel problems with 27-group edits. Notation used in the table is standard. The values of D, $\bar{\Sigma}_a$, and $\bar{\nu}\bar{\Sigma}_f$ are those used in the buckling and reflector savings calculations of Sections V and VI.

TABLE IV. Thermal Parameters Based on Nelkin-kernel THERMOS Problems

Parameter	Lattice												
	B1.27 \square S	B1.27 Δ S	H1.349 \square A	H1.349 \square S	H1.24 \square A	H1.24 \square S	H1.27 Δ A	H1.27 Δ S	H1.166 Δ A	H1.166 Δ S	H1.127 Δ A	H1.127 Δ S	H1.069 Δ S
ρ^{25}	0.82539	0.83604	0.81884	0.74013	0.83605	0.75436	0.84465	0.76139	0.85818	0.77247	0.86278	0.77641	0.78231
ρ_{fuel}	0.89089	0.90259	0.92613	0.83724	0.94602	0.85373	0.95606	0.86196	0.97198	0.87506	0.97749	0.87966	0.88664
ρ_{clad}	0.05849	0.05930	0.00605	0.10009	0.00620	0.10229	0.00627	0.10341	0.00638	0.10511	0.00642	0.10559	0.10603
$\rho_{\text{H}_2\text{O}}$	0.05062	0.03811	0.06782	0.06267	0.04778	0.04398	0.03767	0.03463	0.02164	0.01983	0.01609	0.01475	0.00733
η^{25}	2.0620	2.0593	2.0647	2.0642	2.0619	2.0611	2.0596	2.0588	2.0542	2.0528	2.0506	2.0499	2.0430
η_{fuel}	1.9103	1.9075	1.8256	1.8248	1.8223	1.8212	1.8196	1.8186	1.8137	1.8121	1.8100	1.8093	1.8026
$\bar{\Sigma}_a, \text{cm}^{-1}$	0.18099	0.20076	0.12813	0.13857	0.14254	0.15429	0.14970	0.16288	0.16152	0.17513	0.16328	0.17917	0.18040
$\bar{\nu}\bar{\Sigma}_f, \text{cm}^{-1}$	0.30803	0.34565	0.21663	0.21170	0.24572	0.23990	0.26042	0.25532	0.28473	0.27771	0.28888	0.28517	0.28834
$\bar{\Sigma}_s, \text{cm}^{-1}$	1.7966	1.5948	1.6424	1.7126	1.3753	1.4570	1.2061	1.2991	0.88265	0.99114	0.74730	0.86749	0.66384
$\bar{\Sigma}_{tr}, \text{cm}^{-1}$	1.5654	1.4259	1.3965	1.4727	1.1998	1.2887	1.0757	1.1776	0.84625	0.96414	0.74992	0.88216	0.74699
D, cm	0.2129	0.2338	0.2387	0.2263	0.2778	0.2587	0.3099	0.2831	0.3939	0.3457	0.4445	0.3779	0.4462
\bar{L}^2, cm^2	1.176	1.165	1.863	1.633	1.949	1.677	2.070	1.738	2.439	1.974	2.722	2.109	2.473

Table V compares thermal quantities for three of the lattices, based on the use of Nelkin, free-gas, and Brown-St. John kernels for hydrogen in the THERMOS problems. The three scattering kernels yield close results for most quantities. The Nelkin kernel produces the hardest spectrum of the three kernels; the free-gas kernel gives a scattering cross section that is considerably smaller than that for the other two.

TABLE V. Comparisons of Thermal Quantities Based on Various Scattering Kernels for Hydrogen

Scattering Kernel ^a	Lattice								
	B1.27 Δ S				H1.24 Δ A		H1.127 Δ S		
	Nelkin	Free Gas	Brown-St. John	Nelkin	Free Gas	Brown-St. John	Nelkin	Free Gas	Brown-St. John
$\bar{\theta}_2/\bar{\theta}_1$	1.1150	1.1247	1.1200	1.0894	1.0966	1.0934	1.0772	1.0816	1.0797
$\bar{\theta}_3/\bar{\theta}_1$	1.2535	1.2506	1.2667	1.1572	1.1584	1.1656	1.1367	1.1421	1.1410
\bar{n}_2/\bar{n}_1	1.1590	1.1752	1.1673	1.1230	1.1358	1.1300	1.1057	1.1161	1.1120
\bar{n}_3/\bar{n}_1	1.3554	1.3523	1.3759	1.2184	1.2224	1.2324	1.1858	1.2002	1.1971
\bar{V}_1	1.5900	1.5413	1.5342	1.5788	1.5455	1.5170	1.9374	1.8841	1.8855
\bar{V}_2	1.5295	1.4751	1.4718	1.5314	1.4921	1.4680	1.8874	1.8260	1.8308
\bar{V}_3	1.4703	1.4255	1.4124	1.4995	1.4646	1.4350	1.8572	1.7930	1.7972
$\bar{\epsilon}^2$	0.82539	0.82538	0.82506	0.83605	0.83642	0.83624	0.77641	0.77606	0.77640
$\bar{\epsilon}_{fuel}$	0.89089	0.89062	0.89024	0.94602	0.94599	0.94570	0.87966	0.87894	0.87931
$\bar{\epsilon}_{clad}$	0.05849	0.05908	0.05863	0.00620	0.00625	0.00620	0.10559	0.10619	0.10585
$\bar{\epsilon}_{H2O}$	0.05062	0.05030	0.05113	0.04778	0.04776	0.04810	0.01475	0.01487	0.01484
η^{25}	2.0620	2.0631	2.0633	2.0619	2.0625	2.0633	2.0499	2.0512	2.0511
η_{fuel}	1.9103	1.9119	1.9122	1.8223	1.8236	1.8246	1.8093	1.8112	1.8110
$\bar{\Sigma}_a, \text{cm}^{-1}$	0.18099	0.18758	0.18723	0.14254	0.14594	0.14847	0.17917	0.18458	0.18446
$\bar{\Sigma}_f, \text{cm}^{-1}$	0.30803	0.31941	0.31873	0.24572	0.25176	0.25618	0.28517	0.29383	0.29375
$\bar{\Sigma}_S, \text{cm}^{-1}$	1.7966	1.3181	1.8737	1.3753	1.0177	1.4348	0.86749	0.73341	0.88599

^aSubscripts 1, 2, and 3 denote fuel, cladding, and water regions, respectively.

Table VI lists thermal-flux and neutron-number-density ratios obtained from both 27-group (0-0.415 eV) and 30-group (0-0.785 eV) edits of the Nelkin-kernel problems. Extending the energy range by 0.37 eV does

TABLE VI. Thermal-flux and Neutron-number-density Ratios for 27-group and 30-group Edits

Lattice Groups ^a	B1.27 Δ S		B1.27 Δ S		H1.349 Δ A		H1.349 Δ S		H1.24 Δ A	
	27	30	27	30	27	30	27	30	27	30
$\bar{\theta}_2/\bar{\theta}_1$	1.1150	1.1022	1.1124	1.0980	1.0910	1.0832	1.0837	1.0763	1.0894	1.0802
$\bar{\theta}_3/\bar{\theta}_1$	1.2535	1.2256	1.2299	1.2008	1.1737	1.1589	1.1905	1.1738	1.1572	1.1413
\bar{n}_2/\bar{n}_1	1.1590	1.1520	1.1565	1.1478	1.1242	1.1202	1.1143	1.1105	1.1230	1.1178
\bar{n}_3/\bar{n}_1	1.3554	1.3395	1.3235	1.3055	1.2411	1.2333	1.2648	1.2558	1.2184	1.2093
Lattice Groups ^a	H1.24 Δ S		H1.27 Δ A		H1.27 Δ S		H1.166 Δ A		H1.166 Δ S	
	27	30	27	30	27	30	27	30	27	30
$\bar{\theta}_2/\bar{\theta}_1$	1.0819	1.0731	1.0880	1.0775	1.0807	1.0710	1.0853	1.0727	1.0781	1.0662
$\bar{\theta}_3/\bar{\theta}_1$	1.1709	1.1529	1.1486	1.1315	1.1615	1.1428	1.1286	1.1097	1.1375	1.1170
\bar{n}_2/\bar{n}_1	1.1129	1.1078	1.1218	1.1155	1.1116	1.1057	1.1179	1.1090	1.1077	1.0991
\bar{n}_3/\bar{n}_1	1.2381	1.2275	1.2063	1.1957	1.2246	1.2127	1.1774	1.1641	1.1903	1.1754
Lattice Groups ^a	H1.127 Δ A		H1.127 Δ S		H1.069 Δ S					
	27	30	27	30	27	30				
$\bar{\theta}_2/\bar{\theta}_1$	1.0831	1.0696	1.0772	1.0637	1.0730	1.0581				
$\bar{\theta}_3/\bar{\theta}_1$	1.1271	1.1072	1.1367	1.1143	1.1167	1.0923				
\bar{n}_2/\bar{n}_1	1.1147	1.1044	1.1057	1.0953	1.0986	1.0852				
\bar{n}_3/\bar{n}_1	1.1729	1.1577	1.1858	1.1684	1.1570	1.1353				

^aSubscripts 1, 2, and 3 denote fuel, cladding, and water regions, respectively.

not lower the flux and number-density ratios very much. This suggests that comparisons of experimental and theoretical disadvantage factors (essentially \bar{n}_3/\bar{n}_1) should not be very sensitive to thicknesses of cadmium covers as far as the effect of changing cutoff energy is concerned.

As mentioned above, the slowing-down source term in the THERMOS problems was taken as being due to hydrogen only, and was spatially flat in the H_2O region. For the $H1.069\Delta S$ lattice, a B692/RP problem was run with the source density in each region taken proportional to $\xi\Sigma_S$ of that region. These source densities were 0.01604, 0.01791, and 1.000 in fuel, cladding, and H_2O respectively. Table VII compares fluxes from this problem with those from the problem with source in H_2O only. Table VII also gives B692/RP fluxes for the $H1.069\Delta S$ lattice, obtained by using cross sections for the $H1.127\Delta S$ lattice.

TABLE VII. B692/RP Problems for the $H1.069\Delta S$ Lattice

Flux Ratio ^a	A	B	C
$\bar{\phi}_2/\bar{\phi}_1$	1.0786	1.0713	1.0874
$\bar{\phi}_3/\bar{\phi}_1$	1.1334	1.1194	1.1480

A: Standard problem
B: Source densities proportional to $\xi\Sigma_S$
C: Cross sections for the $H1.127\Delta S$ lattice used.

^aSubscripts 1, 2, and 3 denote fuel, cladding, and water regions, respectively.

As expected, the use of regional source densities proportional to $\xi\Sigma_S$ flattens the flux somewhat in comparison with the case in which the source is in H_2O only. However, the effect for the $H1.069\Delta S$ lattice is not large and would be smaller for all other lattices. The use of $H1.127\Delta S$ cross sections in place of the $H1.069\Delta S$ cross sections increases flux peaking slightly because of the larger absorption cross section for the softer spectrum of the looser lattice. In fact, the flux ratios for the $H1.069\Delta S$ lattice using the $H1.127\Delta S$ cross sections are somewhat higher than the corresponding flux ratios for the $H1.127\Delta S$ lattice, rather than lower, as was the case for the standard problem.

Experimental disadvantage factors were measured in the lattices with stainless steel cladding. The experimental values are ratios of the average subcadmium U^{235} fission-product activity per unit weight of a

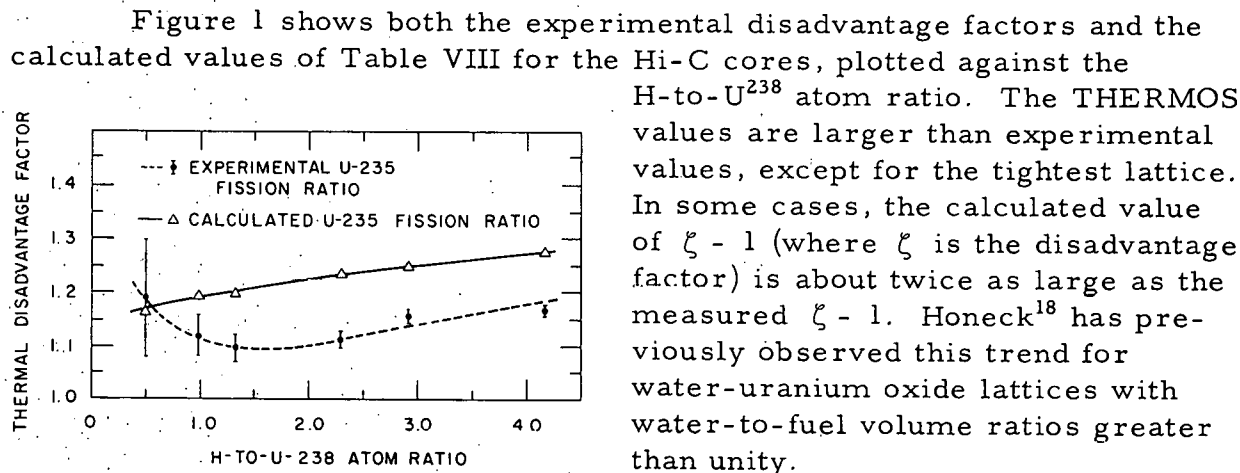
highly enriched foil in the H_2O moderator to that of a highly enriched foil in the fuel. Reference 1 gives details of the experimental techniques and the experimental results.

Table VIII presents U^{235} fission ratios for the stainless steel-clad lattices obtained from 27-group edits of the Nelkin-kernel THERMOS problems. These fission ratios are not greatly different from the corresponding neutron-number-density ratios given in Table III. This is because the fission activation is proportional to $\int \Sigma_f(V) N(V) V dV$, where $\Sigma_f(V)$ is the fission cross section, and $N(V)$ is the neutron number density at velocity V . Since U^{235} is nearly a $1/V$ absorber in the thermal-energy range, the integral is almost proportional to $\int N(V) dV$.

TABLE VIII. U^{235} Fission Ratios for Lattices with Stainless Steel Cladding

Fission Ratios ^a	Lattice							
	B1.27 \square S	B1.27 Δ S	H1.349 \square S	H1.240 \square S	H1.27 Δ S	H1.166 Δ S	H1.127 Δ S	H1.069 Δ S
F_2/F_1	1.1655	1.1629	1.1188	1.1174	1.1162	1.1119	1.1097	1.1021
F_3/F_1	1.3705	1.3372	1.2755	1.2479	1.2337	1.1979	1.1927	1.1624

^aSubscripts 1, 2, and 3 denote fuel, cladding, and water regions, respectively.



112-8069

Fig. 1. Experimental and Theoretical Thermal Disadvantage Factors in Hi-C Cores

yield a disadvantage factor that is monotonically decreasing with decreasing lattice pitch. Weiss and Stamm'ler¹⁹ have shown that the disadvantage factor, calculated in a one-group framework, does not decrease monotonically with decreasing moderator thickness, but possesses a minimum and will increase as the moderator thickness decreases beyond a certain value. These considerations of Weiss and Stamm'ler assume the use of cross sections that are independent of lattice pitch. It was pointed out above, in reference to Table VII, that the B692/RP flux ratios for the H1.069 Δ S lattice, calculated

The experimental results indicate a minimum in the disadvantage factor, whereas calculations

using the $H_1.127\Delta S$ cross sections, are higher than the flux ratios for the $H_1.127\Delta S$ lattice. Thus the progressive hardening of the cross sections with decreasing lattice pitch in the THERMOS problems overbalances the tendency, based on spatial-transport-theory effects, for the disadvantage factor to have a minimum.

The use of a unit cell with the isotropic-return boundary condition may not be very good for the extremely closely packed lattices. Hardy *et al.*²⁰ predicted a minimum for the disadvantage factor in metal lattices using a 36-group Monte Carlo program that treated the cell geometry explicitly. Also, Fukai²¹ pointed out that the cylindrical-cell, isotropic-return boundary condition breaks down somewhat for very tightly packed lattices, in that the disadvantage factor does not increase rapidly enough with decreasing pitch.

Another source of calculational error is the assumption of isotropic scattering. Honeck,¹⁸ however, demonstrated that anisotropic scattering effects are rather small.

A significant effect has been discovered²² in connection with the interpretation of thermal-disadvantage-factor measurements. Three-dimensional Monte Carlo calculations, explicitly including foils, indicate that the flux in a foil is often considerably different from the flux in the medium in which it is placed, even for optically thin foils. The flux peaking or dipping depends strongly on the medium surrounding the foil.

Calculations were carried out²² using a 32-group, thermal Monte Carlo code, DRAM, both for some lattices at Bettis Atomic Power Laboratory and for the Hi-C lattices. Disadvantage factors were computed both for the foil regions and for unperturbed regions in the rod and moderator. For all lattices, the disadvantage factors for the unperturbed regions were higher than those for the foil regions. Disadvantage factors for foil regions were in better agreement with the experimental values than were those for the unperturbed regions. Thus, the results of these calculations explain the fact that calculated disadvantage factors tend to be higher than measured ones.

Disadvantage factors for a small cell represent a severe test of both calculational and experimental techniques. In the case of the calculations, the isotropic-return boundary condition breaks down somewhat for the very tightly packed lattices. The large error bars in Fig. 1 and the discussion in Ref. 1 demonstrate experimental difficulties. Also, the fact that fluxes in foils do not necessarily represent fluxes in the surrounding unperturbed media very well, introduces complications into a comparison of theory and experiment. Thus the discrepancy between experiment and theory shown in Fig. 1 is not surprising.

IV. CALCULATION OF NONTHERMAL PARAMETERS

Parameters for three fast groups with lower boundary energies at 1.35 MeV, 1.23 keV, and 0.414 eV were obtained using the GAM-I code.¹¹ These group limits are such that most U^{238} fission occurs in the first group, and most resonance absorption occurs in the third group. The second group is mainly a slowing-down group, although considerable U^{238} capture does occur in this group.

The GAM-I code calculates fast-neutron spectra and associated multigroup constants using either the P_1 or B_1 approximation. The GAM-I library tape²³ contains data for 68 fine groups, having lethargy widths of $\Delta u = 0.25$, ranging from 10 MeV to 0.414 eV. In the work reported here, the cross sections on the original GAM-I tape were used for hydrogen, oxygen, aluminum, iron, nickel, and chromium. For U^{235} and U^{238} , the cross sections on the original tape led to calculated bucklings that were much higher than experimental. The cross sections of U^{235} and U^{238} were therefore replaced by versions obtained from Hanford, based on the data in Ref. 24. The new U^{238} cross sections differ from the original in the values of σ_C , σ_f , ν , and resonance parameters, with transfer cross sections remaining unchanged. For U^{235} , all cross sections are changed from the original, and resonance parameters are included.

In the GAM-I code, it is assumed that the materials involved form a homogeneous mixture, except for the materials with resonance parameters. For such materials (U^{238} and U^{235} , in our case), the methods of Adler, Hinman, and Nordheim²⁵ are used. Resonance integrals for individual resonances are calculated using either the narrow resonance (NR) or narrow resonance-infinite mass absorber (NRIA) approximation, depending on whether the average energy loss in a collision with the absorber atom is larger or smaller than the practical width.²⁵ The escape probability for the fuel rod is computed using the formula for an isolated rod, the mean chord length, \bar{l} , being replaced by $\bar{l}/(1 - C)$, where C is the Dancoff factor. Dancoff factors for the GAM-I input were determined from the table²⁶ calculated by Carlvik. The cladding, void, and H_2O cross sections were homogenized to yield the moderator cross section used in looking up the Dancoff factors in the table. Since the table involves two parallel rods only, an approximate method was used for determining the effect of shielding by rods intervening between pairs of rods. The contribution for two rods partly shielded by intervening rods was determined by multiplying the C value for the two unshielded rods by d_{\perp}/d . Here d is the rod diameter, while d_{\perp} is defined as follows: Consider a plane cutting the rods perpendicular to the rod axes. Draw a line in the plane joining the axes of the rods for which the Dancoff factor is being calculated. Then draw two more lines in the plane parallel to the first line and tangent to the intervening rods on the sides nearest the first line. The perpendicular distance between these two lines is d_{\perp} . Table IX lists the scattering cross

sections used in the Dancoff-factor determinations. Table X presents the Dancoff factors, calculated as just described, along with values computed by revised versions of the B692/RP collision-probability codes.^{16,17} The two-region version evaluates C from Eq. 17 of Ref. 17; the three-region version uses the three-region extension of Eq. 17, the clad and void regions being homogenized into one region.

TABLE IX. Scattering Cross Sections Used in Dancoff-factor Calculations

Material	σ_p , barns	Material	σ_p , barns
Hydrogen	20.0	Nickel	17.0
Oxygen	3.66	Chromium	4.2
Aluminum	1.42	U^{235}	10.7
Iron	11.0	U^{238}	10.7

TABLE X. Dancoff Factors

Core Code	Ref. 26	B692/RP 2-region	B692/RP 3-region
B1.27□S	0.250	0.22934	0.23418
B1.27△S	0.307	0.29903	0.30413
H1.349□A	0.272	0.25211	0.26688
H1.349□S	0.250	0.22812	0.23518
H1.24□A	0.365	0.35370	0.36910
H1.24□S	0.331	0.31674	0.32405
H1.27△A	0.425	0.42608	0.44094
H1.27△S	0.383	0.37908	0.38610
H1.166△A	0.576	0.58655	0.59809
H1.166△S	0.513	0.51512	0.52049
H1.127△A	0.652	0.66358	0.67280
H1.127△S	0.577	0.57939	0.58365
H1.069△S	0.690	0.69195	0.69407

Three-region values of C from the B692/RP code are a little larger than two-region ones, the largest difference being less than 6%. Differences between three- and two-region values are greater for aluminum-clad fuel than for stainless steel-clad fuel, since the cross section of aluminum differs from that of water by more than the stainless steel cross section does. Comparison of the values based on Carlvik's table and the B692/RP values shows that the Carlvik values tend to be a little lower than those from B692/RP for tight lattices, and a little higher for looser lattices. At any rate, the use of a Dancoff factor as in the GAM-I code implies that the cladding is treated in the narrow-resonance approximation. This may not be very well justified for broad low-lying resonances, especially in the case of stainless steel cladding.

Table XI gives resonance integrals from the GAM-I output for U^{238} absorption and for U^{235} absorption and fission. These values include only contributions from resolved and unresolved resonances and not the contribution from the smoothly varying part of the cross sections. The decrease in the resonance integrals with decreasing lattice pitch is apparent in Table XI, as is the fact that resonance integrals for stainless steel-clad rods are higher than for aluminum-clad rods, especially for the tighter lattices. All the U^{235} resonance integrals are greater than 80% of the corresponding infinite-dilution values, so that U^{235} is not strongly self-shielded even in the tightest lattices.

TABLE XI. Resonance Integrals from GAM-I Output

Core Code	Resonance Integrals, barns		
	U^{238} Absorption	U^{235} Absorption	U^{235} Fission
B1.27□S	19.104	271.48	168.96
B1.27△S	18.253	269.27	167.68
H1.349□A	17.841	282.65	175.51
H1.349□S	18.158	283.29	175.88
H1.24□A	16.686	279.65	173.80
H1.24□S	17.187	280.81	174.46
H1.27△A	15.793	277.42	172.52
H1.27△S	16.418	279.01	173.43
H1.166△A	14.660	270.85	168.79
H1.166△S	15.645	274.14	170.65
H1.127△A	13.297	265.99	166.04
H1.127△S	14.644	270.79	168.75
H1.069△S	12.730	263.10	164.40
Infinite Dilution	273.80	319.70	197.22
Smooth	5.167	92.85	78.33

GAM-I problems were run for all lattices in the P_1 approximation and for most lattices in the B_1 approximation. The input bucklings used were the experimental values of Table XII of Ref. 1 for lattices that went critical without an external driver zone. Estimated values were used for lattices requiring a driver zone to attain criticality. No B_1 problems were run for the two most tightly packed stainless steel-clad Hi-C lattices because the buckling, B^2 , is negative for these lattices, and the B_1 approximation requires $\sqrt{B^2}$ in the input. GAM-I problems were also run for water, using $B^2 = 0.0001 \text{ cm}^{-2}$ in order to obtain parameters for the radial-reflector-savings calculations.

Table XII lists constants from the GAM-I output for the three fast groups in the P_1 approximation. The diffusion equation for a group may be written as

$$D_i \nabla^2 \phi_i - \Sigma_{Ri} \phi_i + \sum_{j < i} \Sigma_{ji} \phi_j + \Sigma_{ii}^{n,2n} \phi_i + \chi_i \sum_j \nu_j \Sigma_{fj} \phi_j = 0. \quad (2)$$

Here Σ_{Ri} equals $\Sigma_{ci} + \Sigma_{fi} + \Sigma_{out i}$, where Σ_{ci} and Σ_{fi} are the capture and fission cross sections in group i ; and $\Sigma_{out i}$, which equals

$$\sum_{j > i} \left(\Sigma_{ij}^{el} + \Sigma_{ij}^{inel} + \Sigma_{ij}^{n,2n} \right),$$

is the total removal cross section from group i by elastic, inelastic, and $(n,2n)$ processes. The transfer cross section Σ_{ij} is given by the sum

$$\Sigma_{ij}^{el} + \Sigma_{ij}^{inel} + 2 \Sigma_{i,j}^{n,2n},$$

and is the total cross section for transfer of neutrons to group j from processes in group i . Other notation used in Eq. 2 is self-explanatory. The group-energy limits used here are such that $\chi_1 = 0.57309$, $\chi_2 = 0.42691$, and $\chi_3 = 0$. The $(n,2n)$ reaction occurs only in group 1, so that $\Sigma_{ii}^{n,2n}$ equals zero for $i \neq 1$.

Table XII shows that scattering other than to the next lower group is quite small, and that the $(n,2n)$ reaction contributes little. Capture and fission processes in group 3 and fast fission in group 1 are all quite important.

Table XIII compares P_1 and B_1 constants for two lattices. The constants from the two approximations are almost the same, except for the diffusion constants. This is because the diffusion constants involve current weighting with the fine-group currents in GAM-I, whereas the other quantities are computed using flux weighting. The differences between P_1 and B_1 constants are greater for the $B1.27\Delta S$ lattice than for the $H1.127\Delta A$ lattice since the input B^2 values were 0.010734 and 0.0010 cm^{-2} , respectively. In the limit of zero buckling, the P_1 and B_1 equations become identical.

TABLE XII. Constants from GAM-I for Three Fast Groups in the P_1 Approximation

Parameter	Lattice													
	B1.27 Δ S	B1.27 Δ S	H1.349 Δ A	H1.349 Δ S	H1.24 Δ A	H1.24 Δ S	H1.27 Δ A	H1.27 Δ S	H1.166 Δ A	H1.166 Δ S	H1.127 Δ A	H1.127 Δ S	H1.069 Δ S	Water
D ₁ , cm	2.0344	2.0137	2.1606	2.0555	2.1574	2.0329	2.1560	2.0195	2.1545	1.9918	2.1544	1.9816	1.9650	2.2472
D ₂ , cm	0.99514	0.98236	1.0400	1.0011	1.0327	0.98756	1.0284	0.97895	1.0213	0.96468	1.0182	0.95582	0.94040	1.0949
D ₃ , cm	0.54907	0.54839	0.62441	0.55454	0.64206	0.55603	0.65600	0.55814	0.69110	0.56509	0.70964	0.56859	0.57373	0.59511
$\Sigma R_1, \text{cm}^{-1}$	0.095708	0.093294	0.089762	0.092912	0.085808	0.089600	0.083185	0.087374	0.077776	0.082802	0.075318	0.080653	0.076920	0.10706
$\Sigma R_2, \text{cm}^{-1}$	0.061156	0.055170	0.057226	0.058104	0.049412	0.050223	0.044338	0.045158	0.033911	0.034374	0.029183	0.029775	0.021455	0.10422
$\Sigma R_3, \text{cm}^{-1}$	0.11529	0.10632	0.10465	0.10642	0.092159	0.094145	0.083691	0.085887	0.066173	0.068647	0.057406	0.060371	0.045569	0.17149
$v_1 \Sigma f_1, \text{cm}^{-1}$	0.012514	0.014418	0.012409	0.012404	0.014650	0.014629	0.016097	0.016064	0.019018	0.018939	0.020320	0.020225	0.022341	0
$v_2 \Sigma f_2, \text{cm}^{-1}$	0.0022992	0.0026493	0.0015432	0.0015415	0.0018155	0.0018126	0.0019891	0.0019854	0.0023356	0.0023278	0.0024884	0.0024792	0.0027329	0
$v_3 \Sigma f_3, \text{cm}^{-1}$	0.026415	0.029738	0.017296	0.017343	0.019910	0.019975	0.021438	0.021523	0.023805	0.023908	0.024420	0.024574	0.024322	0
$\Sigma_{11}^{n,2n}, \text{cm}^{-1}$	0.62516×10^{-4}	0.70911×10^{-4}	0.64271×10^{-4}	0.65222×10^{-4}	0.74340×10^{-4}	0.74821×10^{-4}	0.80425×10^{-4}	0.80622×10^{-4}	0.91118×10^{-4}	0.389893×10^{-4}	0.95037×10^{-4}	0.93674×10^{-4}	0.97840×10^{-4}	0
$\Sigma_{12}, \text{cm}^{-1}$	0.090169	0.087023	0.084260	0.087421	0.079445	0.083256	0.076264	0.080477	0.069725	0.074970	0.066759	0.072139	0.067572	0.10617
$\Sigma_{13}, \text{cm}^{-1}$	0.53238×10^{-4}	0.46942×10^{-4}	0.49377×10^{-4}	0.49635×10^{-4}	0.41200×10^{-4}	0.41542×10^{-4}	0.35832×10^{-4}	0.36210×10^{-4}	0.24812×10^{-4}	0.25251×10^{-4}	0.19816×10^{-4}	0.20237×10^{-4}	0.11632×10^{-4}	0.90140×10^{-4}
$\Sigma_{14}, \text{cm}^{-1}$	0.17830×10^{-7}	0.15707×10^{-7}	0.16532×10^{-7}	0.16618×10^{-7}	0.13775×10^{-7}	0.13889×10^{-7}	0.11966×10^{-7}	0.12092×10^{-7}	0.82507×10^{-8}	0.33965×10^{-8}	0.65664×10^{-8}	0.67062×10^{-8}	0.33048×10^{-8}	0.30277×10^{-7}
$\Sigma_{23}, \text{cm}^{-1}$	0.057060	0.050435	0.053469	0.054250	0.044956	0.045652	0.039419	0.040110	0.028018	0.028346	0.022824	0.023257	0.014056	0.10418
$\Sigma_{24}, \text{cm}^{-1}$	0.18712×10^{-4}	0.16472×10^{-4}	0.17538×10^{-4}	0.17757×10^{-4}	0.14665×10^{-4}	0.14849×10^{-4}	0.12796×10^{-4}	0.12973×10^{-4}	0.89442×10^{-5}	0.39950×10^{-5}	0.71880×10^{-5}	0.72671×10^{-5}	0.41537×10^{-5}	0.34615×10^{-4}
$\Sigma_{34}, \text{cm}^{-1}$	0.080037	0.067591	0.076403	0.076802	0.060995	0.061223	0.051229	0.051386	0.031821	0.031564	0.023747	0.023463	0.010572	0.17029

TABLE XIII. A Comparison of P_1 and B_1 Constants from GAM-I

Parameter	B1.27 Δ S		H1.127 Δ A	
	B ₁	P ₁	B ₁	P ₁
D ₁ , cm	1.8904	2.0344	2.1367	2.1544
D ₂ , cm	0.97309	0.99514	1.0159	1.0182
D ₃ , cm	0.54655	0.54907	0.70892	0.70964
$\Sigma R_1, \text{cm}^{-1}$	0.095523	0.095708	0.075316	0.075318
$\Sigma R_2, \text{cm}^{-1}$	0.061179	0.061156	0.029183	0.029183
$\Sigma R_3, \text{cm}^{-1}$	0.11530	0.11529	0.057406	0.057406
$v_1 \Sigma f_1, \text{cm}^{-1}$	0.012532	0.012514	0.020321	0.020320
$v_2 \Sigma f_2, \text{cm}^{-1}$	0.0022993	0.0022992	0.0024884	0.0024884
$v_3 \Sigma f_3, \text{cm}^{-1}$	0.026415	0.026415	0.024420	0.024420
$\Sigma_{11}^{n,2n}, \text{cm}^{-1}$	0.63838×10^{-4}	0.62516×10^{-4}	0.95059×10^{-4}	0.95037×10^{-4}
$\Sigma_{12}, \text{cm}^{-1}$	0.089974	0.090169	0.066757	0.066759
$\Sigma_{13}, \text{cm}^{-1}$	0.53104×10^{-4}	0.53238×10^{-4}	0.19815×10^{-4}	0.19316×10^{-4}
$\Sigma_{14}, \text{cm}^{-1}$	0.17785×10^{-7}	0.17830×10^{-7}	0.65661×10^{-8}	0.65664×10^{-8}
$\Sigma_{23}, \text{cm}^{-1}$	0.057082	0.057060	0.022825	0.022824
$\Sigma_{24}, \text{cm}^{-1}$	0.18719×10^{-4}	0.18712×10^{-4}	0.71882×10^{-5}	0.71380×10^{-5}
$\Sigma_{34}, \text{cm}^{-1}$	0.080045	0.080037	0.023747	0.023747

V. CRITICALITY CALCULATIONS

A FORTRAN code, BUCKLE, was written for the CDC-160A computer to calculate critical bucklings and fluxes by fundamental-mode methods. This code uses the set of equations, Eq. 2, with $\nabla^2\phi_i$ replaced by $-B^2\phi_i$. The quantity

$$\sum_j \nu_j \sum_{fj} \phi_j$$

is set equal to unity, and values of ϕ_1 , ϕ_2 , ..., are calculated in turn using an input value of B^2 . Then the process is repeated for other values of B^2 until

$$\sum_j \nu_j \sum_{fj} \phi_j$$

calculated using the computed fluxes, is equal to unity within an input-convergence criterion.

Calculations using BUCKLE were done for all lattices using the P_1 constants of Table XII for the three fast groups, and the constants of Table IV for the thermal group. Experimental values, where available, were used for the input buckling. Problems were also run using the B_1 constants for the three fast groups. Table XIV gives the results of these calculations. Here B_m^2 is the material buckling from BUCKLE, and B_g^2 is the experimental geometric buckling from Table XII of Ref. 1. The quantity k_{eff} is defined by

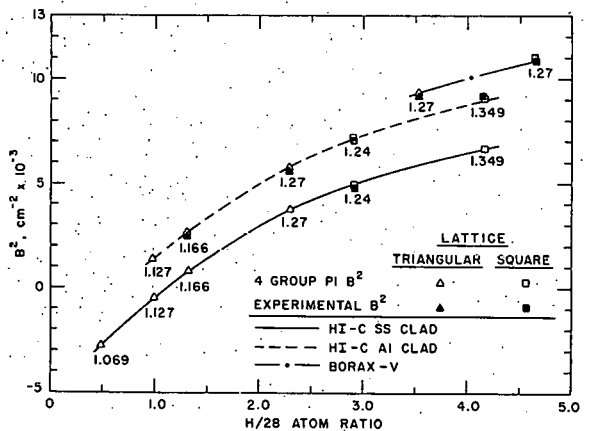
$$k_{eff} = \sum_j \nu_j \sum_{fj} \phi_j$$

Figure 2 shows the calculated bucklings, based on the P_1 approximation in GAM-I, along with the experimental bucklings.

The calculated bucklings are higher than the experimental ones, except for the H1.349□A lattice in the P_1 approximation. The average values of k_{eff} for the lattices that went critical without a driver zone are 1.0044 and 1.0107 for the P_1 and B_1 cases, respectively.

TABLE XIV. Bucklings and Fluxes from Fundamental-mode Calculations

Core Code	GAM-I Option	GAM-I						
		B_m^2 , cm^{-2}	B_g^2 , cm^{-2}	$k_{\text{eff}}(B_g^2)$	ϕ_1	ϕ_2	ϕ_3	ϕ_4
B1.27 \square S	P_1	0.010873	0.010734	1.0038	4.8664	12.0277	5.6619	2.4734
	B_1	0.011270		1.0143	4.9081	12.0382	5.6597	2.4716
B1.27 Δ S	P_1	0.009301	0.009147	1.0045	5.1191	13.5659	6.1429	2.0471
	B_1	0.009589		1.0127	5.1514	13.5730	6.1401	2.0457
H1.349 \square A	P_1	0.008994	0.009182	0.9940	5.2514	13.0579	6.3343	3.7166
	B_1	0.009303		1.0038	5.2951	13.0692	6.3322	3.7137
H1.349 \square S	P_1	0.006635		-	5.3819	13.8602	6.8319	3.7477
	B_1	0.006792		-	5.4019	13.8654	6.8308	3.7464
H1.24 \square A	P_1	0.007111	0.007076	1.0013	5.6699	15.4584	7.1872	3.0351
	B_1	0.007302		1.0079	5.7007	15.4655	7.1844	3.0331
III.24 \square S	P_1	0.004968	0.004747	1.0076	5.7526	16.4314	7.7432	3.0487
	B_1	0.005052		1.0104	5.7645	16.4343	7.7420	3.0479
H1.27 Δ A	P_1	0.005777	0.005538	1.0094	5.9972	17.5876	7.9275	2.6823
	B_1	0.005899		1.0140	6.0191	17.5922	7.9248	2.6809
H1.27 Δ S	P_1	0.003764		-	6.0392	18.6911	8.5230	2.6729
	B_1	0.003807		-	6.0457	18.6923	8.5221	2.6725
H1.166 Δ A	P_1	0.002649	0.002436	1.0105	6.8723	24.7451	10.1977	1.9975
	B_1	0.002674		1.0117	6.8780	24.7454	10.1962	1.9972
H1.166 Δ S	P_1	0.000752		-	6.8054	26.6636	10.9447	1.9710
	B_1	0.000756		-	6.8063	26.6630	10.9446	1.9710
H1.127 Δ A	P_1	0.001380		-	7.3288	29.9514	11.7110	1.6982
	B_1	0.001386		-	7.3301	29.9508	11.7106	1.6981
H1.127 Δ S	P_1	-0.000480		-	7.1989	32.2765	12.4929	1.6390
H1.069 Δ S	P_1	-0.002773		-	8.0295	51.4392	16.4428	0.97145

Fig. 2
Theoretical and Experimental Bucklings

112-8007

Table XV gives the parameters involved in the two-group criticality equation used in the analysis of Brookhaven light-water-moderated lattices.²⁷ This equation is

$$\frac{(\eta f)_1(1 - p_1)}{1 + \tau B^2} + \frac{(\eta f)_2 p_1}{(1 + \tau B^2)(1 + L^2 B^2)} = 1, \quad (3)$$

where the subscripts 1 and 2 designate fast and thermal groups, respectively, and the definitions used are

$$(\eta f)_1 = \frac{\nu_1 \Sigma f_1}{\Sigma'_{a1}}, \quad (\eta f)_2 = \frac{\nu_2 \Sigma f_2}{\Sigma_{a2}}, \quad p_1 = \frac{\Sigma_{12}}{\Sigma'_{a1} + \Sigma_{12}},$$

$$\Sigma'_{a1} = \Sigma_{a1} - \Sigma_{11}^{n,2n}, \quad \tau = \frac{D_1}{\Sigma'_{a1} + \Sigma_{12}}, \quad \text{and} \quad L^2 = \frac{D_2}{\Sigma_{a2}}.$$

These definitions differ slightly from those used in the Brookhaven work in that the $(n, 2n)$ reaction was not considered there. The fast-group constants involved in Table XV are based on the one-group edits of the GAM-I problems; the thermal constants are based on Table IV. Values of B^2 in Table XV are slightly different from the B_m^2 in Table XIV, since two-group and four-group bucklings would agree only if the exact theoretical critical buckling was used in the GAM-I input.

TABLE XV. Two-group Parameters

Parameter	B1.27ΔS	B1.27ΔS	H1.349ΔA	H1.349ΔS	H1.24ΔA	H1.24ΔS	H1.27ΔA	H1.27ΔS
p_1	0.62246	0.55482	0.65399	0.64865	0.57211	0.56485	0.51405	0.50566
$(\eta f)_1$	0.86548	0.87682	0.76138	0.72618	0.77482	0.73432	0.78359	0.73886
$(\eta f)_2$	1.7019	1.7217	1.6907	1.5278	1.7239	1.5549	1.7396	1.5675
τ, cm^2	34.266	36.026	39.066	35.460	42.785	38.311	45.706	40.469
L^2, cm^2	1.1763	1.1646	1.8630	1.6331	1.9489	1.6767	2.0701	1.7381
B^2, cm^{-2}	0.010879	0.009309	0.008983	0.006641	0.007113	0.004974	0.005787	0.003775
λ_1^a	0.2380	0.2923	0.1950	0.2065	0.2542	0.2684	0.3012	0.3169
λ_2^a	0.7620	0.7077	0.8050	0.7935	0.7458	0.7316	0.6988	0.6831
Parameter	H1.166ΔA	H1.166ΔS	H1.127ΔA	H1.127ΔS	H1.069ΔS			
p_1	0.37130	0.35721	0.30155	0.28620	0.14425			
$(\eta f)_1$	0.78282	0.73204	0.78684	0.72781	0.70016			
$(\eta f)_2$	1.7628	1.5857	1.7692	1.5916	1.5983			
τ, cm^2	53.729	47.396	58.787	50.932	61.316			
L^2, cm^2	2.4387	1.9740	2.7223	2.1092	2.4734			
B^2, cm^{-2}	0.002652	0.000763	0.001379	-0.000481	-0.002751			
λ_1^a	0.4308	0.4541	0.5084	0.5326	0.7207			
λ_2^a	0.5692	0.5459	0.4916	0.4674	0.2793			

^a λ_1 and λ_2 are the first and second terms of the left member of Eq. 3, representing fast and thermal fissions, respectively.

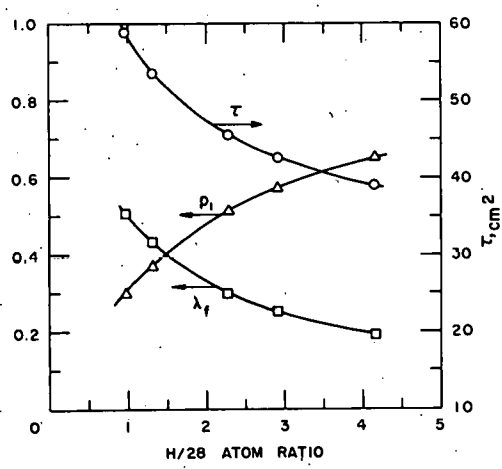


Table XV shows clearly the increasing importance of nonthermal events as the water-to-fuel ratio is decreased, the parameters p_1 and λ_1 being especially significant. Figure 3 shows the variation of p_1 , λ_1 , and τ with H-to-U²³⁸ ratio for the aluminum-clad Hi-C lattices.

Fig. 3. Two-group Parameters for Hi-C Aluminum-clad Lattices

VI. RADIAL REFLECTOR SAVINGS

Radial reflector savings were calculated for the seven lattices that went critical without an external driver zone. The multigroup, one-dimensional, diffusion-theory code, RP-122 (REX), was used. Both four-group and two-group computations were carried out using both P_1 and B_1 nonthermal constants from GAM-I and thermal constants from THERMOS. To determine criticality, the REX code iterates on the axial buckling, B_Z^2 . The critical B_Z^2 from the REX output was subtracted from the BUCKLE value of B_m^2 to obtain the radial buckling, B_R^2 . Hence the radial reflector savings, λ_R , were found from

$$\lambda_R = \frac{2.4048}{B_R} - R.$$

The core radii used in the REX problems were essentially those of the experiments. A convergence criterion was used such that k_{eff} for the converged B_Z^2 differs from unity by less than 0.0001. Table XVI compares the calculated values of λ_R with experimental results from Table XII of Ref. 1.

TABLE XVI. Radial Reflector Savings

Core Code	Reflector Savings, cm				
	Four-group		Two-group		
	P_1	B_1	P_1	B_1	Experimental
B1.27□S	7.21	6.95	7.30	7.04	7.35 ± 0.27
B1.27△S	7.57	7.35	7.63	7.40	7.55 ± 0.10
H1.24□S	7.76	7.64	7.69	7.58	7.69 ± 0.08
H1.349□A	7.73	7.48	7.81	7.56	7.38 ± 0.12
H1.24□A	8.45	8.25	8.46	8.25	8.13 ± 0.16
H1.27△A	9.02	8.85	8.94	8.76	8.77 ± 0.17
H1.166△A	10.86	10.72	10.32	10.23	10.73 ± 0.14

reverse situation is true. The four-group values of λ_R involving P_1 constants agree with experimental values within the quoted experimental error in four cases out of seven.

No axial reflector savings were calculated because of the complicated structure of the bottom reflector, which consists of Lucite and water. Also, λ_R is of more interest than λ_Z because the radial buckling contributes considerably more to the experimental B_g^2 than does the axial buckling.

Values of λ_R using P_1 constants are always higher than the corresponding B_1 values. In some cases, a four-group calculation yields a larger λ_R than a two-group calculation; in other cases, the

VII. MICROPARAMETER CALCULATIONS

A. Initial and Modified Conversion Ratios and α^{25}

The initial conversion ratio (ICR) is defined as the ratio of the captures in U^{238} to absorptions in U^{235} in a fresh core and so represents the ratio of Pu^{239} production to U^{235} destruction. The modified conversion ratio (MCR) is the ratio of U^{238} captures to U^{235} fissions and is more closely related to what was actually measured in the experiments.¹ The parameter α^{25} is the ratio of captures to fissions in U^{235} . Thus the relation $ICR = MCR/(1 + \alpha^{25})$ is true.

Table XVII presents values of ICR, MCR, and α^{25} calculated using the P_1 cross sections from GAM-I and the thermal cross sections from the THERMOS Nelkin-kernel problems. Use of the B_1 parameters from GAM-I would make little difference in the results. In Table XVII, C_f^{28} and C_t^{28} are the fast and thermal captures in U^{238} , respectively. The term "fast" refers to processes in the three GAM-I groups; "thermal" refers to those in the THERMOS groups. Likewise, A_f^{25} , A_t^{25} , C_f^{25} , C_t^{25} , F_f^{25} , F_t^{25} , α_f^{25} , and α_t^{25} refer to absorptions, captures, fissions, and α in fast and thermal-energy ranges for U^{235} .

TABLE XVII. Initial and Modified Conversion Ratios and α^{25}

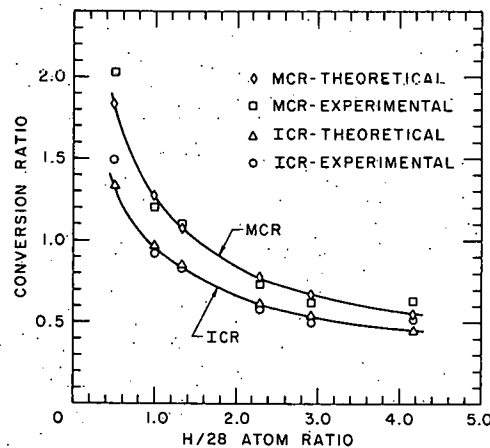
Parameter	Lattice												
	B1.27DS	B1.27AS	H1.349DA	H1.349DS	H1.24DA	H1.24DS	H1.27DA	H1.27AS	H1.166DA	H1.166AS	H1.127DA	H1.127AS	H1.069AS
C_f^{28}	0.13402	0.16156	0.14687	0.15991	0.18728	0.20521	0.21829	0.24008	0.31390	0.35113	0.36685	0.41474	0.60034
C_t^{28}	0.02932	0.02735	0.05109	0.05043	0.04758	0.04674	0.04474	0.04378	0.03672	0.03541	0.03181	0.03032	0.01828
A_f^{25}	0.10846	0.13367	0.07883	0.08502	0.10388	0.11201	0.12427	0.13383	0.18176	0.19592	0.21762	0.23394	0.32499
A_t^{25}	0.36949	0.34360	0.38994	0.38436	0.36169	0.35484	0.33916	0.33148	0.27688	0.26664	0.23923	0.22800	0.13710
C_f^{25}	0.034240	0.042183	0.025105	0.027141	0.033056	0.035746	0.039524	0.042725	0.057680	0.062519	0.068898	0.074568	0.10288
C_t^{25}	0.055956	0.052415	0.058619	0.057860	0.054790	0.053868	0.051698	0.050637	0.042819	0.041391	0.037351	0.035664	0.021835
F_f^{25}	0.074215	0.091493	0.053724	0.057880	0.070826	0.076253	0.084744	0.091106	0.12409	0.13340	0.14872	0.15938	0.22211
F_t^{25}	0.31353	0.29118	0.33132	0.32650	0.30691	0.30097	0.28746	0.28084	0.23406	0.22525	0.20188	0.19234	0.11527
α_f^{25}	0.4614	0.4611	0.4673	0.4689	0.4667	0.4689	0.4664	0.4690	0.4648	0.4687	0.4633	0.4679	0.4632
α_t^{25}	0.1785	0.1800	0.1769	0.1772	0.1785	0.1790	0.1798	0.1803	0.1829	0.1838	0.1850	0.1854	0.1894
ICR	0.3418	0.3958	0.4223	0.4481	0.5045	0.5397	0.5676	0.6100	0.7645	0.8357	0.8726	0.9635	1.3387
MCR	0.4213	0.4937	0.5141	0.5472	0.6218	0.6679	0.7067	0.7632	0.9790	1.0778	1.1371	1.2654	1.8336
α^{25}	0.2326	0.2472	0.2174	0.2211	0.2326	0.2376	0.2451	0.2510	0.2806	0.2897	0.3031	0.3134	0.3697

Table XVIII compares experimental and calculated conversion ratios for all lattices for which experiments were performed. The experimental values are from Table XIX of Ref. 1. Values of α^{25} used in deriving the experimental ICR from the experimental MCR are slightly different from the values in Table XVII. The conversion ratios in Table XVIII for the Hi-C cores are also plotted against the H-to- U^{238} atom ratio in Fig. 4.

Agreement between theory and experiment in the case of the conversion ratios is reasonably good. The initial conversion ratio is greater than unity only for the tightest lattice, which has a negative buckling.

TABLE XVIII. Calculated and Experimental Conversion Ratios

Lattice	Calculated		Experimental	
	MCR	ICR	MCR	ICR
B1.27□S	0.4213	0.3418	0.367 ± 0.018	0.297 ± 0.015
B1.27△S	0.4937	0.3958	0.413 ± 0.021	0.330 ± 0.016
H1.349□S	0.5472	0.4481	0.635 ± 0.007	0.518 ± 0.006
H1.24□S	0.6679	0.5397	0.622 ± 0.006	0.500 ± 0.005
H1.27△S	0.7632	0.6100	0.730 ± 0.021	0.581 ± 0.017
H1.166△S	1.0778	0.8357	1.082 ± 0.006	0.835 ± 0.005
H1.127△S	1.2654	0.9635	1.203 ± 0.025	0.913 ± 0.019
H1.069△S	1.8336	1.3387	2.023 ± 0.047	1.485 ± 0.034



112-6731

Fig. 4. Conversion Ratios for Hi-C Stainless Steel-clad Cores

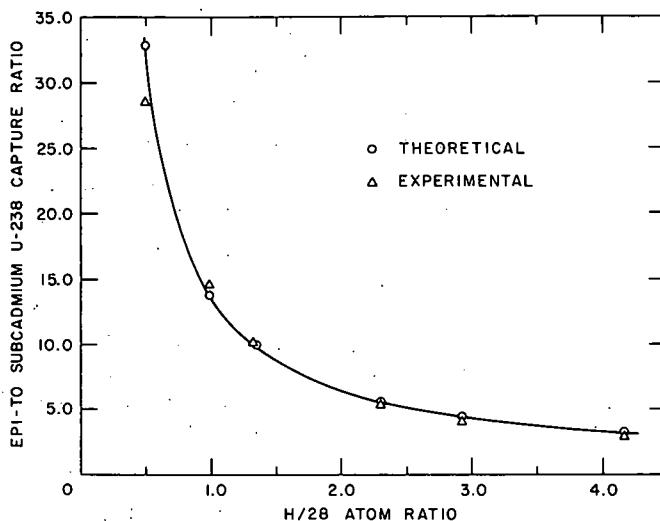
B. U^{238} Capture Cadmium Ratios

Experimental U^{238} capture cadmium ratios were measured for the lattices with stainless steel cladding. Values were also calculated for all the lattices on the assumption that captures in the three GAM-I groups represent epicadmium capture, and captures in the THERMOS group represent subcadmium capture. Thus no consideration was given as to whether the experimental cadmium cutoff energies were in agreement with the 0.414-eV lower limit of the GAM-I calculations. Table XIX presents both calculated and experimental values.

TABLE XIX. Calculated and Experimental U^{238} Capture Cadmium Ratios

Lattice	Calculated		Experimental	
	CR^{28}	ρ^{28}	CR^{28}	ρ^{28}
B1.27□S	1.2188	4.571	1.182 ± 0.041	5.49 ± 1.24
B1.27△S	1.1693	5.907	1.188 ± 0.083	5.32 ± 2.35
H1.349□A	1.3479	2.875	-	-
H1.349□S	1.3154	3.171	1.328 ± 0.004	3.05 ± 0.04
H1.24□A	1.2541	3.936	-	-
H1.24□S	1.2278	4.390	1.243 ± 0.002	4.12 ± 0.03
H1.27△A	1.2050	4.879	-	-
H1.27△S	1.1824	5.484	1.185 ± 0.003	5.40 ± 0.09
H1.166△A	1.1170	8.548	-	-
H1.166△S	1.1008	9.916	1.100 ± 0.001	10.0 ± 0.1
H1.127△A	1.0867	11.53	-	-
H1.127△S	1.0731	13.68	1.069 ± 0.002	14.5 ± 0.4
H1.069△S	1.0304	32.84	1.035 ± 0.001	28.6 ± 0.8

The experimental values are from Table XX of Ref. 1. In Table XIX, CR^{28} is the U^{238} capture cadmium ratio, while ρ^{28} is the epicadmium-to-subcadmium capture ratio. Thus, $\rho^{28} = 1/(CR^{28} - 1)$. Figure 5 is a plot of experimental and theoretical values of ρ^{28} versus the H-to-U²³⁸ atom ratio for the Hi-C stainless steel-clad cores. Satisfactory agreement exists between theory and experiment.



112-6732

Fig. 5. U^{238} Epicadmium to Subcadmium Capture Ratios for Hi-C Stainless Steel-clad Cores

of U^{235} fission cadmium ratio versus H-to- U^{238} atom ratio falls on essentially a straight line, as suggested in Ref. 7, although the slopes of the theoretical and experimental lines are somewhat different.

C. U^{235} Fission Cadmium Ratios

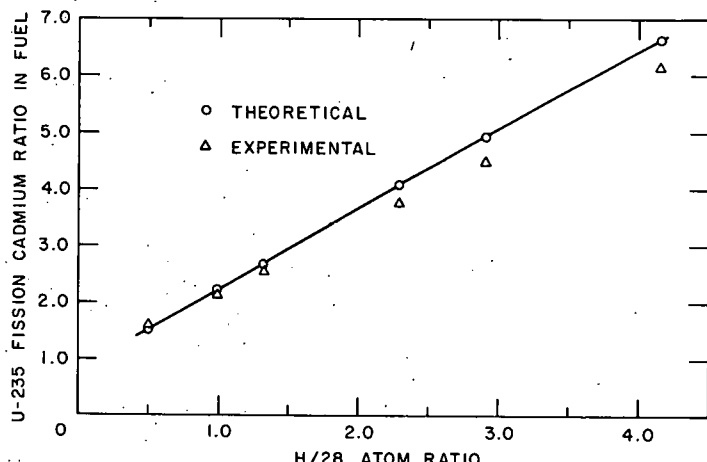
Fission cadmium ratios, CR_f^{25} , were measured for the stainless steel-clad lattices. As for the U^{238} capture cadmium ratios, U^{235} fission cadmium ratios were calculated on the assumption that the GAM-I groups and the THERMOS group correspond to epicadmium and subcadmium energy ranges, respectively. Table XX presents experimental values from Table XXIII of Ref. 1 along with calculated values. Figure 6 shows the data in graphical form for the Hi-C stainless steel-clad cores. The data in the plot

TABLE XX. Calculated and Experimental U^{235} Fission Cadmium Ratios

Lattice	Calculated CR_f^{25}	Experimental CR_f^{25}	Lattice	Calculated CR_f^{25}	Experimental CR_f^{25}
B1.27□S	5.225	4.94 ± 0.20	H1.27△A	4.392	-
B1.27△S	4.183	3.90 ± 0.16	H1.27△S	4.083	3.75 ± 0.08
H1.349□A	7.167	-	H1.166△A	2.886	-
H1.349□S	6.641	6.13 ± 0.20	H1.166△S	2.689	2.55 ± 0.06
H1.24□A	5.333	-	H1.127△A	2.357	-
H1.24□S	4.947	4.49 ± 0.11	H1.127△S	2.207	2.15 ± 0.05
			H1.069△S	1.519	1.59 ± 0.03

D. Gold and Indium Cadmium Ratios

Both gold and indium cadmium ratios were measured in almost all the lattices. Calculated values were obtained using the B512/RP foil-activation program.²⁸



112-8006

Fig. 6. U^{235} Fission Cadmium Ratios for Hi-C Stainless Steel-clad Cores

covers. The flux has the energy dependence of a Maxwellian plus a $1/E$ tail. More specifically, the energy dependence is given by

$$\phi(X) = \frac{2r}{\sqrt{\pi}} X e^{-X} + \frac{X_0^{1/2}}{X} \Delta(X), \quad (4)$$

where r is a constant, $X = E/E_M$, $X_0 = E_{2200}/E_M$, and $\Delta(X)$ is zero for $X < \mu$ and unity for $X \geq \mu$. Here, E is the neutron energy, E_M is the energy at the peak of the Maxwellian, and E_{2200} is the energy corresponding to a neutron velocity of 2200 m/sec. In most of the calculations, the parameter μ was taken to be 5. Scattering by the foil and covers is neglected, so that their cross sections represent absorption only. The energy dependence of the cross sections is a sum of single-level Breit-Wigner resonances without Doppler broadening and a $1/V$ component. For cadmium and indium, the cross sections were considered to be given completely by the resonances at 0.178 and 1.457 eV, respectively. For gold, a $1/V$ component yielding a cross section of 5.05 barns at 0.0253 eV was added to the cross section produced by the 4.906 eV resonance. The resonance parameters used are from Ref. 15.

Values of E_M were determined, using output from the THERMOS calculations, from the maxima in the plots of the neutron number density per unit velocity, $N(V)$, versus the velocity. Plots using the $N(V)$ at the fuel center and at the outer mesh interval in H_2O were assumed to be adequate to represent the fuel and water regions, respectively. The values of r were found by equating the ratio ϕ_4/ϕ_3 to the ratio of the integral of the flux of Eq. 4 over the energy range of the THERMOS group to the corresponding integral over the energy range of the third GAM-I group. Here ϕ_4 and ϕ_3 are the fluxes determined by the fundamental-mode calculations, ϕ_4 being adjusted to yield the average flux in fuel or H_2O , rather than in the unit cell.

The B512/RP program calculates both the neutron absorption in a bare foil of thickness t and the absorption in the same foil between two identical covers (usually cadmium) of thickness ℓ_0 in slab geometry. The cadmium cut-off energy, E_{cut} , is also computed. Flux depression in the foil and covers, resulting from neutron absorption, is considered. The flux is assumed to impinge isotropically on the outer surface of the bare foil or on the outer surface of the

The experimental-foil thicknesses were 1.1, 1.2, and 20 mils for gold, indium, and cadmium, respectively. Tables XXI and XXII present results of the calculations for gold and indium, respectively, along with experimental values from Table XXV of Ref. 1.

TABLE XXI. Gold Cadmium Ratios

Lattice	Region	E _M , eV	r	E _{cut} , eV	CR	
					Calculated	Experimental
B1.27□S	Fuel ^a	0.0415	1.625	0.5309	1.378	1.413 ± 0.025
B1.27□S	H ₂ O	0.0323	2.250	0.5869	1.525	1.520 ± 0.045
B1.27△S	Fuel ^a	0.0434	1.170	0.5323	1.286	1.288 ± 0.030
B1.27△S	H ₂ O	0.0352	1.553	0.5873	1.382	1.354 ± 0.040
H1.349□A	Fuel	0.0370	2.537	0.5863	1.572	1.62 ± 0.02
H1.349□S	Fuel	0.0377	2.305	0.5864	1.525	1.58 ± 0.02
H1.24□A	Fuel	0.0402	1.693	0.5866	1.401	1.455 ± 0.008
H1.24□A	Fuel ^b	0.0402	1.334	0.5870	1.373	1.455 ± 0.008
H1.24□A	Fuel ^c	0.0402	2.181	0.6085	1.454	1.455 ± 0.008
H1.24□A	Fuel ^d	0.0402	1.693	0.7298	1.139	
H1.24□A	H ₂ O	0.0346	2.085	0.5869	1.488	1.503 ± 0.015
H1.24□S	Fuel	0.0408	1.534	0.5867	1.369	1.435 ± 0.008
H1.24□S	H ₂ O	0.0346	1.917	0.5870	1.455	1.442 ± 0.008
H1.27△A	Fuel	0.0421	1.277	0.5868	1.316	1.361 ± 0.015
H1.27△S	Fuel	0.0428	1.146	0.5869	1.289	1.346 ± 0.015
H1.166△A	Fuel	0.0489	0.618	0.5869	1.175	1.221 ± 0.008
H1.166△S	Fuel	0.0496	0.546	0.5870	1.160	1.201 ± 0.005
H1.127△A	Fuel	0.0517	0.399	0.5872	1.128	1.177 ± 0.010
H1.127△S	Fuel	0.0525	0.340	0.5873	1.115	1.152 ± 0.015
H1.069△S	Fuel	0.0600	0.0793	0.5888	1.055	1.099 ± 0.008

^a15-mil, rather than 20 mil, cadmium covers.

^b $\mu = 3$, rather than 5.

^c $\mu = 10$, rather than 5.

^dFoil thickness, t = 0.

TABLE XXII. Indium Cadmium Ratios

Lattice	Region	E _M , eV	r	E _{cut} , eV	CR	
					Calculated	Experimental
B1.27□S	Fuel ^a	0.0415	1.625	0.6757	1.416	1.470 ± 0.020
B1.27□S	H ₂ O	0.0323	2.250	0.7623	1.570	1.558 ± 0.040
B1.27△S	Fuel ^a	0.0434	1.170	0.6764	1.326	1.382 ± 0.030
B1.27△S	H ₂ O	0.0352	1.553	0.7625	1.433	1.412 ± 0.040
H1.349□A	Fuel	0.0370	2.537	0.7619	1.619	1.61 ± 0.03
H1.349□S	Fuel	0.0377	2.305	0.7620	1.574	1.58 ± 0.03
H1.24□A	Fuel	0.0402	1.693	0.7620	1.453	1.482 ± 0.015
H1.24□A	Fuel ^b	0.0402	1.334	0.7623	1.430	1.482 ± 0.015
H1.24□A	Fuel ^c	0.0402	2.181	0.7764	1.493	1.482 ± 0.015
H1.24□A	Fuel ^d	0.0402	1.693	1.203	1.222	
H1.24□A	H ₂ O	0.0346	2.085	0.7623	1.536	1.518 ± 0.020
H1.24□S	Fuel	0.0408	1.534	0.7621	1.422	1.469 ± 0.008
H1.24□S	H ₂ O	0.0346	1.917	0.7624	1.503	1.483 ± 0.020
H1.27△A	Fuel	0.0421	1.277	0.7621	1.369	1.398 ± 0.015
H1.27△S	Fuel	0.0428	1.146	0.7621	1.343	1.373 ± 0.007
H1.166△A	Fuel	0.0489	0.618	0.7620	1.231	1.260 ± 0.008
H1.166△S	Fuel	0.0496	0.546	0.7621	1.216	1.234 ± 0.005
H1.127△A	Fuel	0.0517	0.399	0.7621	1.184	1.204 ± 0.020
H1.127△S	Fuel	0.0525	0.340	0.7622	1.171	
H1.069△S	Fuel	0.0600	0.0793	0.7632	1.108	1.135 ± 0.008

^a15-mil, rather than 20-mil, cadmium covers.

^b $\mu = 3$, rather than 5.

^c $\mu = 10$, rather than 5.

^dFoil thickness, t = 0.

The calculated gold cadmium ratios are usually somewhat lower than the experimental ones, the discrepancy becoming greater as the lattice pitch is decreased. Calculated values of CR-1 are about 10% too low for the looser Hi-C lattices and 45% too low for the tightest lattice. Agreement between theory and experiment is a little better for indium, although the trend of calculated values being too low for tightly packed lattices continues. The value of CR-1 for indium in the tightest lattice is only about 20% too low. The effect of flux depression in the gold or indium foils is quite important, even for the thin foils used here, since the cross sections of the dominant resonances are very large. This effect is seen by comparing the calculated cadmium ratios of the H1.24□A lattice for the actual value of $t = 20$ mils and for $t = 0$.

The calculations described here have a number of deficiencies. The treatment of the energy dependence of the flux as a Maxwellian plus a $1/E$ tail is not very accurate. There is some departure from Maxwellian behavior, especially for the tighter lattices. The high absorption causes the tail to depart from the $1/E$ form. Also, the cutoff of $\mu = 5$ is not strongly justified. An idea of the effect of changing μ is obtained by comparing the cadmium ratios for $\mu = 3, 5$, and 10 for the H1.24□A lattice in Tables XXI and XXII. The consideration of the flux at the center of the fuel and at the outer mesh interval in H_2O as being representative of fuel and H_2O average values is also approximate.

Other calculational deficiencies include the use of only one resonance in representing the cross sections, the neglect of Doppler broadening, and the neglect of scattering by the foils. In view of the approximate nature of the calculations, the discrepancies between theory and experiment are not surprising.

E. U^{238} -to- U^{235} Fission Ratios

The ratio of the number of fissions in U^{238} to those in U^{235} can be calculated from the GAM-I and THERMOS cross sections, along with the fluxes from BUCKLE, as

$$\delta^{28} = \frac{N^{28} \sum_{i=1}^4 \sigma_{fi}^{28} \phi_i}{N^{25} \sum_{i=1}^4 \sigma_{fi}^{25} \phi_i} \quad (5)$$

Most of the contribution to the numerator in Eq. 5 comes from Group 1, none coming from below Group 2.

An approximate formula for δ^{28} may be derived as follows. The diffusion equation for Group 1 is

$$D_1 \nabla^2 \phi_1 - \sum R_1 \phi_1 + \sum_{11}^{n,2n} \phi_1 + \chi_1 \nu_1 \sum f_1 \phi_1 + \chi_1 \sum_{i=2}^4 \nu_i \sum f_i \phi_i = 0, \quad (6)$$

where the notation is as in Eq. 2. On using $\nabla^2 \phi_1 = -B^2 \phi_1$, we can rewrite Eq. 6 as

$$\phi_1 = \frac{\chi_1 \sum_{i=2}^4 \nu_i \sum f_i \phi_i}{\sum R_1 - \sum_{11}^{n,2n} - \chi_1 \nu_1 \sum f_1 + D_1 B^2} \quad (7)$$

Now make the following approximations:

1. All U^{238} fissions occur in Group 1.
2. All U^{235} fissions occur below Group 1, except that U^{235} Group 1 fissions are included in the $\chi_1 \nu_1 \sum f_1$ terms in the denominator of Eq. 7.
3. For U^{235} fission, $\nu_2 = \nu_3 = \nu_4 = \nu_t = 2.43$.

These approximations lead to the equation

$$\delta^{28} = \frac{\nu_t \chi_1 \sum f_1^{28}}{\sum R_1 - \sum_{11}^{n,2n} - \chi_1 \nu_1 \sum f_1 + D_1 B^2} \quad (8)$$

Equation 8 has the advantage of involving only Group 1 cross sections. The first of the above three approximations is the poorest, causing the values of δ^{28} given by Eq. 8 to be a few percent too low.

Values of δ^{28} were calculated for all the lattices using Eq. 5. Also, approximate values were computed from Eq. 8 using three sets of cross sections. These were the Group 1 cross sections from the GAM-I output, and cross sections obtained by averaging the first eight fine groups, having lethargy widths of 0.25, of the GAM-I (Ref. 23) and MUFT-4 (Ref. 29) libraries over a U^{235} fission spectrum. In the case of the GAM-I library, the versions of U^{235} and U^{238} from Hanford were used, as mentioned in Section IV above.

The calculations outlined above were done in the homogeneous approximation; that is, no allowance was made for the spatial variation of the fast flux in the unit cell. This is reasonably well justified in the energy

region of importance for fast fission since the cross sections are relatively small, and the mean free paths are therefore long. To study heterogeneous effects, average fluxes were calculated for the three regions (fuel, cladding, and water) of the unit cell with the B692/RP collision-probability code.^{16,17} Both GAM-I and MUFT-4 fission-spectrum-averaged cross sections were used. The transport approximation was used for elastic scattering. Average regional fluxes from B692/RP were combined with the cross sections for the individual cell regions to yield homogenized constants for Eq. 8.

Table XXIII presents values of δ^{28} , calculated by all the methods described above, along with the experimental values measured for lattices with stainless steel cladding. The experimental values are from Table XXI of Ref. 1. Figure 7 shows the experimental and calculated four-group values of δ^{28} for the Hi-C stainless steel-clad cores. The GAM-I and MUFT-4 cross sections, averaged over a fission spectrum from 1.35 to 10 MeV, are presented in Tables XXIV and XXV, respectively. Table XXVI gives the average fluxes in Group 1, calculated using the GAM-I fission-spectrum cross sections.

TABLE XXIII. U²³⁸-to-U²³⁵ Fission Ratios

Method	Lattice												
	B1.27 Δ S	B1.27 Δ A	H1.349 Δ A	H1.349 Δ S	H1.24 Δ A	H1.24 Δ S	H1.27 Δ A	H1.27 Δ S	H1.166 Δ A	H1.166 Δ S	H1.127 Δ A	H1.127 Δ S	H1.069 Δ S
Four-group GAM-I (P ₁ , homogeneous)	0.05424	0.06674	0.06136	0.06302	0.07991	0.08121	0.09440	0.09513	0.1334	0.1320	0.1555	0.1524	0.1971
Four-group GAM-I (P ₁ , heterogeneous) ^a	0.05686	0.06908	0.06419	0.06606	0.08230	0.08379	0.09649	0.09742	0.1349	0.1337	0.1566	0.1537	0.1979
One-group GAM-I (P ₁ , homogeneous)	0.05132	0.06309	0.05794	0.05945	0.07535	0.07644	0.08892	0.08943	0.1253	0.1234	0.1459	0.1422	0.1827
One-group GAM-I (fission spectrum, homogeneous)	0.05373	0.06630	0.06056	0.06213	0.07909	0.08040	0.09363	0.09447	0.1327	0.1317	0.1551	0.1525	0.1977
One-group GAM-I (fission spectrum, heterogeneous)	0.05633	0.06862	0.06336	0.06513	0.08146	0.08295	0.09570	0.09674	0.1342	0.1334	0.1562	0.1538	0.1985
One-group MUFT-4 (fission spectrum, homogeneous)	0.05564	0.06914	0.06304	0.06489	0.08323	0.08486	0.09942	0.1006	0.1448	0.1437	0.1717	0.1685	0.2255
One-group MUFT-4 (fission spectrum, heterogeneous)	0.05837	0.07159	0.06603	0.06814	0.08579	0.08767	0.1017	0.1031	0.1465	0.1456	0.1731	0.1701	0.2266
Experimental	0.0650 ± 0.006	0.1190 ± 0.010	-	0.0742 ± 0.0011	-	0.1011 ± 0.0004	-	0.1160 ± 0.0017	-	0.1539 ± 0.0039	0.1889 ± 0.0131	0.1877 ± 0.0020	0.2622 ± 0.0036

^aApproximate four-group heterogeneous values were calculated by multiplying the four-group homogeneous values by the ratio of the δ^{28} value for the one-group, GAM-I, fission-spectrum heterogeneous case to that for the corresponding homogeneous case.

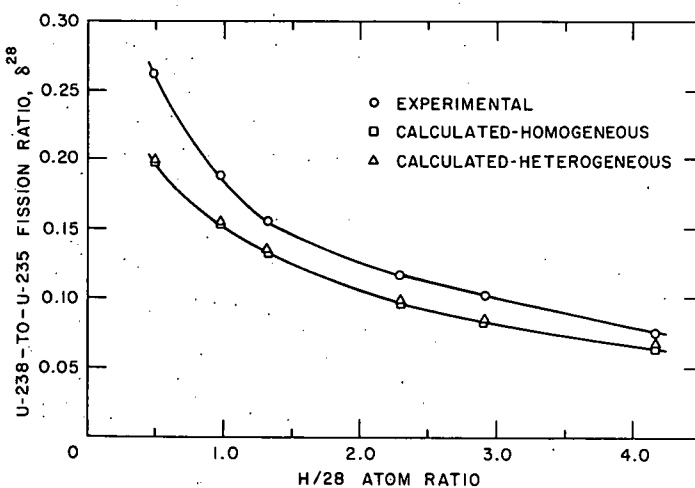


Fig. 7
U²³⁸-to-U²³⁵ Fission Ratios
for Hi-C Stainless Steel-clad Cores

TABLE XXIV. GAM-I Cross Sections Averaged over a Fission Spectrum from 1.35 to 10 MeV

Type of Cross Section	Cross Sections, barns							
	Hydrogen	Oxygen	Aluminum	Iron	Nickel	Chromium	^{238}U	^{235}U
σ_c	0	0.0208	0.00610	0.00166	0.00197	0.0020	0.0355	0.0506
σ_f	0	0	0	0	0	0	0.5149	1.276
$\nu\sigma_f$	0	0	0	0	0	0	1.395	3.598
σ_{inel}^{out}	0	0.00188	0.238	0.650	0.522	0.336	2.307	1.557
σ_{out}^{el}	1.515	0.221	0.118	0.043	0.062	0.062	0.019	0.021
$\sigma_{out}^{n,2n}$	0	0	0	0	0	0	0.0167	0.0075
σ_{11}^{inel}	0	0.00169	0.188	0.348	0.392	0.311	0.261	0.209
$\sigma_{11}^{el}(P_0)$	0.9642	1.7297	2.2903	2.1321	2.3411	2.6850	4.684	4.391
$\sigma_{11}^{el}(P_1)$	2.4809	1.1287	2.7950	2.9436	2.6780	3.3635	8.937	4.031
$\sigma_{11}^{el}(tr)$	0.1372	1.337	1.359	1.151	1.448	1.564	1.705	3.047
$\sigma_{11}^{n,2n}$	0	0	0	0	0	0	0.0082	0.0042

TABLE XXV. MUFT-4 Cross Sections Averaged over a Fission Spectrum from 1.35 to 10 MeV

TABLE XXVI. Average Group 1 Fluxes Calculated Using
GAM-I Fission-spectrum Cross Sections

Lattice	$\bar{\phi}_2/\bar{\phi}_1$ (a)	$\bar{\phi}_3/\bar{\phi}_1$ (a)	Lattice	$\bar{\phi}_2/\bar{\phi}_1$ (a)	$\bar{\phi}_3/\bar{\phi}_1$ (a)
B1.27□S	0.95910	0.93577	H1.27△A	0.97486	0.96243
B1.27△S	0.96655	0.94961	H1.27△S	0.97185	0.96009
H1.349□A	0.95991	0.93682	H1.166△A	0.98355	0.97615
H1.349□S	0.95700	0.93450	H1.166△S	0.98047	0.97372
H1.24□A	0.96968	0.95383	H1.127△A	0.98688	0.98118
H1.24□S	0.96671	0.95150	H1.127△S	0.98376	0.97869
			H1.069△S	0.98883	0.98609

(a) Subscripts 1, 2, and 3 denote fuel, cladding, and water regions, respectively.

Table XXIII and Fig. 7 show that heterogeneous effects on δ^{28} are small and become smaller as the lattice pitch is decreased, as would be expected from the results in Table XXVI. The heterogeneous δ^{28} is less than 5% larger than the corresponding homogeneous value, even for the loosest lattice. One-group values of δ^{28} are smaller than four-group values, as anticipated above, because of the neglect of U^{238} fission below 1.35 MeV. Averaging GAM-I cross sections over a fission spectrum results in δ^{28} values somewhat above those obtained using cross sections averaged over the spectrum generated by GAM-I. This is because the value of ΣR_1 for the GAM-I spectrum is larger than the corresponding fission-spectrum value. MUFT-4 values of δ^{28} are higher than the corresponding GAM-I values. The smaller MUFT-4 inelastic-scattering cross section for U^{238} , seen by comparing Tables XXIV and XXV, is mainly responsible for this.

Since all experimental values are considerably higher than the corresponding theoretical values, it is apparent that agreement between theory and experiment on δ^{28} is not good. The reason for the discrepancy is not known. It may be caused by inadequacies in the cross sections or by some systematic experimental error. In investigating a very tight lattice of 1.3% enrichment, the workers at Westinghouse³⁰ also found that the greatest discrepancy between theory and experiment was in δ^{28} .

Computations were made to determine the reactivity effects of using heterogeneous rather than homogeneous cross sections in Group 1, and also of using MUFT-4 rather than GAM-I cross sections in Group 1. Fast constants obtained using both GAM-I and MUFT-4 fission-spectrum cross sections in both homogeneous and heterogeneous calculations were substituted for the original GAM-I P_1 constants in the first group of the four-group BUCKLE problems. Results for the three lattices studied are presented in Table XXVII in terms of reactivity differences.

TABLE XXVII. Reactivity Changes on Substitution of Various Group 1 Cross Sections into Four-group BUCKLE Problems

Substitution	Reactivity Changes, %		
	B1.27 Δ S	H1.127 Δ A	H1.069 Δ S
GAM-I homogeneous \rightarrow			
GAM-I heterogeneous	+0.134	+0.059	+0.045
MUFT-4 homogeneous \rightarrow			
MUFT-4 heterogeneous	+0.104	+0.063	+0.052
GAM-I homogeneous \rightarrow			
MUFT-4 homogeneous	-1.579	-0.749	+0.702

Table XXVII shows that use of heterogeneous rather than homogeneous cross sections increases reactivity by little more than 0.1%, even for one of the looser lattices. Thus, the use of homogeneous constants in the criticality calculations of Section V is justified. Use of MUFT-4 cross sections in place of GAM-I cross sections decreases reactivity for most lattices, but increases it for the H1.069 Δ S lattice. Section VIII presents a more systematic study of the effects on reactivity of changing important cross sections.

VIII. EFFECTS OF CROSS-SECTION CHANGES ON REACTIVITY

It was mentioned in Section IV that use of the original GAM-I library cross sections for U^{235} and U^{238} led to calculated bucklings that were much higher than experimental ones, and that versions of U^{235} and U^{238} obtained from Hanford were therefore substituted for the original ones. To investigate reactivity effects of cross-section changes, calculations were done, using the BUCKLE code described in Section V, in which certain cross sections were changed by 10%, the others being kept constant. The standard cross sections are those in Tables IV and XII. Table XXVIII presents results in terms of $\Delta k_{\text{eff}}/k_{\text{eff}}$, where k_{eff} is unity for the critical buckling determined by the standard cross sections. No cross-section changes were considered in the thermal group, since thermal cross sections are rather well known. The effects of the indicated cross-section changes on the diffusion coefficients were not treated.

TABLE XXVIII. Effects of Cross-section Changes
on Reactivity ($\Delta k_{\text{eff}}/k_{\text{eff}}$, %)

Lattice	Cross Section with +10% Change						
	Σ_{c1}	Σ_{f1}	$\Sigma_{\text{out}}^{\text{out}}$ Σ_{12}	σ_{c2}^{28}	σ_{c3}^{28}	σ_{c3}^{25}	σ_{f3}^{25}
B1.27□S	-0.047	+0.393	+0.597	-0.367	-1.311	-0.415	+0.667
B1.27△S	-0.051	+0.473	+0.444	-0.468	-1.502	-0.495	+0.832
H1.349□A	-0.049	+0.420	+0.537	-0.410	-1.399	-0.301	+0.499
H1.349□S	-0.052	+0.424	+0.303	-0.424	-1.422	-0.301	+0.586
H1.24□A	-0.057	+0.529	+0.331	-0.561	-1.676	-0.382	+0.669
H1.24□S	-0.062	+0.524	+0.086	-0.583	-1.718	-0.386	+0.780
H1.27△A	-0.067	+0.604	+0.162	-0.693	-1.852	-0.449	+0.807
H1.27△S	-0.065	+0.600	+0.080	-0.714	-1.901	-0.446	+0.944
H1.166△A	-0.083	+0.795	-0.305	-1.098	-2.282	-0.599	+1.225
H1.166△S	-0.082	+0.773	-0.559	-1.149	-2.385	-0.594	+1.423
H1.127△A	-0.090	+0.894	-0.549	-1.385	-2.401	-0.682	+1.478
H1.127△S	-0.091	+0.862	-0.802	-1.462	-2.544	-0.674	+1.708
H1.069△S	-0.111	+1.026	-1.333	-2.487	-2.790	-0.808	+2.339

Table XXVIII shows that the calculated reactivities are quite sensitive to nonthermal cross-section changes in general, the sensitivity increasing as the pitch is decreased and the lattices become more undermoderated. As might be expected, the sensitivity to the U^{238} capture cross section is quite pronounced. The major reason for the large reactivity differences obtained by substitution of the Hanford cross sections is that the original GAM-I cross sections yield values of σ_{c2}^{28} only about half as large as those based on the Hanford cross sections. Table XXVIII shows that such a difference represents a reactivity change of the order of 5% for the H1.166△A lattice. Although the reactivity is even more sensitive to σ_{c3}^{28} than to σ_{c2}^{28} , the differences between Hanford and original GAM-I values of σ_{c3}^{28} are small and therefore do not contribute much to the large reactivity differences.

IX. DISCUSSION AND CONCLUSIONS

Agreement between theory and experiment for the Hi-C and BORAX-V lattices is in general reasonably good, except for δ^{28} . The Hi-C lattices provide a severe test of calculational methods. This is because the close spacing of the fuel rods makes theoretical treatment difficult in general and accurate treatment of nonthermal events quite important. Several improvements could be made in the theoretical methods, although those used should be reasonably good. Some possible improvements are discussed below.

In the thermal-energy region, the use of the isotropic return boundary condition, as mocked up by an extra scattering region at the outer boundary of a circular unit cell, may not be very good for the most tightly packed lattices. A Monte Carlo calculation using the actual square or hexagonal cell would be better than this one-dimensional THERMOS calculation. Other defects in the thermal calculations are the use of isotropic scattering, the treatment of the flux above the thermal cutoff as $1/E$, and the treatment of the slowing-down source as being due to hydrogen only. Also, the prescription used for the calculation of the thermal diffusion coefficient is rather rough. The revised version of THERMOS,³¹ in which the thermal-diffusion coefficient is calculated more accurately, was not available when the calculations reported here were made.

In the resonance region, a treatment of resonance absorption involving neither the extreme NR nor NRIA approximations but using numerical integration of the transport equation would be an improvement. Another possibility would be the use of a Monte Carlo code. Such treatments could also allow for interference effects between resonances lying close together. Another approximation involved is the use, in the resonance calculations, of the escape probability for an isolated rod with the mean chord length, \bar{l} , replaced by $\bar{l}/(1 - C)$, where C is the Dancoff factor. The worst feature of this approximation is probably that the clad is treated in the narrow-resonance approximation in the calculation of the Dancoff factor. This may not be well justified for broad, low-lying resonances, especially for stainless steel-clad rods. Another resonance-region inaccuracy is caused by the fact that all absorption in a given resonance is assigned to the fine GAM-I group in which the resonance energy lies. The treatment of resonance absorption in the unresolved region in GAM-I is also rather approximate. In the case of fissionable isotopes, the Breit-Wigner single-level formula is not adequate, although parameters for multilevel formulas are available only over small-energy ranges. This makes accurate treatment of resonance absorption in U^{235} difficult.

The reason for the large discrepancy between theory and experiment in the case of δ^{28} is not understood. The existence of inaccuracies in the high-energy cross-section data would seem to be the most plausible explanation, although a systematic experimental error is also possible. The reactivity of the Hi-C lattices is quite sensitive to changes in cross sections, as

was shown in Section VIII. The rather good agreement between theory and experiment on reactivity may be a result of cancellations of errors arising both from inaccurate cross sections and from the use of approximate theoretical techniques. Such errors might tend to cancel well in the calculation of reactivity, but not as well in the calculation of another quantity, such as δ^{28} .

The Hi-C program extended investigations of $\text{UO}_2\text{-H}_2\text{O}$ lattices into a range of lower hydrogen-to- U^{238} atom ratios than had been studied previously. Such investigations are of interest because reactors with high conversion ratios and consequently high burnup are expected to become increasingly important in the utilization of nuclear energy. Experimental studies with fuel rods of enrichments other than the nominal 3% used here would also be of interest.

REFERENCES

1. A. R. Boynton, Q. L. Baird, K. E. Plumlee, W. C. Redman, W. R. Robinson, and G. S. Stanford, *High Conversion Critical Experiments*, ANL-7203 (Jan 1967).
2. Q. L. Baird and A. R. Boynton, *Bucklings, Disadvantage Factors and δ^{28} Measurements in Some Undermoderated Slightly Enriched Cores*, Trans. Am. Nucl. Soc. 6, No. 2, 248 (1963).
3. Q. L. Baird, A. R. Boynton, W. R. Robinson, and J. M. Christenson, *Initial Conversion Ratio and Epicadmium to Subcadmium Uranium-238 Capture Ratio Measurements in Very Undermoderated Slightly Enriched Oxide Cores*, Trans. Am. Nucl. Soc. 7, No. 1, 80 (1964).
4. A. R. Boynton, Q. L. Baird, J. M. Christenson, K. E. Plumlee, W. C. Redman, W. R. Robinson, and G. S. Stanford, "High Conversion Critical Experiment," *Reactor Physics Division Annual Report - July 1, 1963 to June 30, 1964*, ANL-7010 (Jan 1965), pp. 33-43.
5. A. R. Boynton, K. E. Plumlee, W. C. Redman, W. R. Robinson, and G. S. Stanford, "High Conversion Critical Experiment," *Reactor Physics Division Annual Report - July 1, 1964 to June 30, 1965*, ANL-7110 (Dec 1965), pp. 82-84.
6. A. R. Boynton, *Thermal Disadvantage Factors in Very Undermoderated Water-Uranium Oxide Lattices*, Nucl. Sci. Eng. 23, 393-395 (1965).
7. G. S. Stanford and K. E. Plumlee, *Linear Relationship Between Cadmium Ratio and Reactor Core Composition*, Trans. Am. Nucl. Soc. 8, No. 1, 270 (1965).
8. E. M. Pennington, "Hi-C Uniform Lattice Calculations," *Reactor Physics Division Annual Report - July 1, 1963 to June 30, 1964*, ANL-7010 (Jan 1965) pp. 44-46.
9. E. M. Pennington, "Hi-C Uniform Lattice Calculations," *Reactor Physics Division Annual Report - July 1, 1964 to June 30, 1965*, ANL-7110 (Dec 1965), pp. 84-90.
10. A. R. Boynton and E. M. Pennington, *Critical Experiments and Calculations in Some Very Undermoderated, Slightly Enriched, Uranium Oxide-Water Lattices*, Trans. Am. Nucl. Soc. 9, No. 1 (1966).
11. G. D. Joanou and J. S. Dudek, *GAM-I: A Consistent P_1 Multigroup Code for the Calculation of Fast Neutron Spectra and Multigroup Constants*, GA-1850 (June 1961).
12. H. C. Honeck, *THERMOS, A Thermalization Transport Code for Reactor Lattice Calculations*, BNL-5826 (Sept 1961).
13. D. A. Newmarch, *Errors Due to the Cylindrical Cell Approximation in Lattice Calculations*, AEEW-R-34 (June 1960).
14. H. C. Honeck, *Some Methods for Improving the Cylindrical Reflecting Boundary Condition in Cell Calculations of the Thermal Neutron Flux*, Trans. Am. Nucl. Soc. 5, No. 2, 350 (1962).
15. D. J. Hughes and R. B. Schwartz, *Neutron Cross Sections*, BNL-325, Second Edition (July 1, 1958); D. J. Hughes, B. A. Magurno, and M. K. Brussel, *Neutron Cross Sections*, BNL-325, Second Edition, Supplement No. 1 (Jan. 1, 1960).

16. E. M. Pennington, *Cylindrical Lattice Collision Probability Codes*, B692/RP, ANL-6836 (Feb 1964).
17. E. M. Pennington, *Collision Probabilities in Cylindrical Lattices*, Nucl. Sci. Eng. 19, 215 (1964).
18. H. C. Honeck, *The Calculation of the Thermal Utilization and Disadvantage Factor in Uranium/Water Lattices*, Nucl. Sci. Eng. 18, 49 (1964).
19. Z. Weiss and R. J. J. Stamm'ler, *Calculation of Disadvantage Factors for Small Cells*, Nucl. Sci. Eng. 19, 374 (1964).
20. J. Hardy, Jr., et al., *Thermal Neutron Spectral and Spatial Distributions in Light Water Moderated Uranium Lattices*, WAPD-T-1594 (1963).
21. Y. Fukai, *On the Disadvantage Factor in a Closely Packed Cylindrical Lattice*, J. Nucl. Sci. Technol. (Tokyo), 3(4), 165 (April 1966).
22. F. E. Dunn, *Flux Dipping and Peaking in Foils Used in Thermal Disadvantage Factor Measurements*, Trans. Am. Nucl. Soc. 9, No. 1, 189 (1966).
23. G. D. Joanou et al., *Nuclear Data for GAM-I Data Tape*, GA-2451, Vol. I, II, III (Aug 1961).
24. R. C. Liikala, *Updated RBU Basic Library*, HW-75716, Vol. 1, 2, 3 (May 20, 1963).
25. F. T. Adler, G. W. Hinman, and L. W. Nordheim, *The Quantitative Evaluation of Resonance Integrals*, Proc. 1958 Geneva Conference 16, Paper No. 1988, pp. 155-171.
26. *Reactor Physics Constants*, ANL-5800, Second Edition (July 1963), Table 4-25.
27. R. L. Hellens and H. C. Honeck, *A Summary and Preliminary Analysis of the BNL Slightly Enriched Uranium, Water Moderated Lattice Measurements*, Technical Reports Series No. 12: Light Water Lattices; International Atomic Energy Agency, Vienna (1962).
28. E. M. Pennington and W. L. Boettinger, *Foil Activation Programs*, B512/RP, ANL-6822 (Jan 1964).
29. A. F. Henry, *54 Group Library for P-1 Programs*, WAPD-TM-224 (April 1960).
30. W. Baer et al., *Study of a Slightly Enriched UO_2 Lattice with H:U = 0.42 - Measurement and Analysis*, Nucl. Sci. Eng. 23, 361 (1965).
31. B. J. Toppel and I. Baksys, *The Argonne-revised THERMOS Code*, ANL-7023 (March 1965).

